MARMARA UNIVERSITY
INSTITUTE FOR GRADUATE STUDIES IN PURE AND APPLIED SCIENCES

Analysis of a Multi-Agent System with Social Value Orientation

Alp Merzi

Ph.D. Thesis

Department of Electrical and Electronics Engineering

Thesis Supervisor

Prof. Dr. Veysel Gazi

ISTANBUL, 2025

MARMARA UNIVERSITY
INSTITUTE FOR GRADUATE STUDIES IN PURE AND APPLIED SCIENCES

Analysis of a Multi-Agent System with Social Value Orientation

Alp Merzi
725017007

Ph.D. Thesis

Department of Electrical and Electronics Engineering

Thesis Supervisor
Prof. Dr. Veysel Gazi

ISTANBUL, 2025

ACKNOWLEDGEMENTS

Despite the unexpected hardships that life throws at us and the times when I found myself in seemingly bottomless dark pits filled with sorrow, completing this dissertation was made possible through the unwavering and sincere support of Prof. Dr. Veysel Gazi, to whom I am deeply grateful.

I would also like to extend my sincere thanks to Prof. Dr. Mehmet Akar for his constructive criticism and to Assoc. Prof. Dr. Onur Cihan, who never hesitated to guide me whenever I faced difficulties.

Of course, my heartfelt gratitude goes to my beloved family, who never withheld their support: my father, Nuri Merzi, my mother, Serpil Özaloğlu, and my dear wife, Gözde Merzi.

Finally, I would like to express my appreciation to the Council of Higher Education (YÖK) for supporting me through the 100/2000 YÖK Doctoral Scholarship program for four years.

February 2025 **Alp Merzi**

TABLE OF CONTENTS

Preface/Acknowledgements i

Özet iv

Abstract v

Claim for Originality vi

List of Figures x

List of Tables xii

1 Introduction 1
- 1.1 Aim of the Study . . . 1
- 1.2 Overview of the Study . . . 3
- 1.3 Literature Review . . . 6

2 Application of SVO to a Target Capturing Problem 15
- 2.1 Problem Definiton . . . 17
  - 2.1.1 Analysis of the Target Capturing with Uncertain Data and Varying Personalities Problem . . . 22
- 2.2 Quadcopter Model . . . 27
  - 2.2.1 quadcopter Model and Control . . . 27
- 2.3 Simulation Results . . . 35
  - 2.3.1 Example 1: Stationary Target . . . 36
  - 2.3.2 Example 2: Mobile Target . . . 40

3 SVO with Coordinate Coupling Matrices for Swarm Formation 46
- 3.1 Problem Formulation . . . 47

3.1.1 Interaction Model 47
3.1.2 Graph Representation of Swarm 48
3.2 Influence of SVO on Swarm's Spatial Arrangement 49
3.2.1 First Example 49
3.2.1.1 Attractive Force 50
3.2.1.2 Repulsive Force 50
3.2.1.3 Simulation Results and Discussion 51
3.2.2 Second Example 55
3.2.2.1 Repulsive Force 55
3.2.2.2 Simulation Results and Discussion 57
3.3 Influence of SVO on Swarm's Rotational Behavior 60
3.3.1 Rotational Behavior Through Skew-Symmetric Matrices 60
3.3.2 Coupling Skew-Symmetric Matrices with SVO 62
3.3.3 Third Example 63
3.3.4 Conclusion on Frequency Analysis 66

4 Conclusion **67**

Bibliography **70**

ÖZET

Sosyal Değer Yönelimli Çok Etmenli Bir Sistemin Analizi

Çok etkenli (multi-agent) sistemlerin, biyolojik, robotik veya fiziksel olmayan toplulukların koordinasyonu ve kontrolü, son otuz yılda kapsamlı bir şekilde incelenmiştir. Çoğu araştırma, ajanlar arasında homojenlik varsayımına dayanırken, gerçek dünya sistemleri genellikle farklı etkileşimlere ve önceliklere sahip davranışsal heterojenlikle karakterize edilir. Bu tez, bireylerin kişisel çıkar ve kolektif sonuçlar arasındaki tercihlerini yansıtan psikolojik bir kavram olan Sosyal Değer Yönelimi'ni (SVO), sürü (swarm) sistemlerinde davranışsal heterojenliği modellemek ve analiz etmek için yeni bir parametre olarak tanıtmaktadır.

SVO'nun çok etkenli koordinasyon çerçevelerine entegre edilmesiyle, bu çalışma SVO'nun sürü dinamikleri üzerindeki etkisini iki uygulama aracılığıyla incelemektedir. İlk uygulama, ajanların SVO değerlerine göre bireysel performans ve grup uyumu arasında denge kurduğu, quadcopter dinamiklerini içeren bir hedef yakalama görevine odaklanmaktadır. Bencil ajanlar, hedefe hızlı bir şekilde ulaşmayı önceliklendirirken; prososyal ajanlar, sürü uyumunu korumayı ön planda tutar. Bu durum, farklı yakınsama davranışlarına yol açar. İkinci uygulama ise, SVO'nun kullanılarak ızgara benzeri durağan oluşumlar ve farklı açısal hızların üretildiği oluşum kontrolü ve dönme hareketlerini ele almaktadır. Bu uygulamalar, SVO'nun mekansal düzenlemeleri, ortaya çıkan davranışları ve sistem performansını çeşitli senaryolarda nasıl etkilediğini göstermektedir.

Bu araştırma, sosyal psikolojinin teorik modelleri ile çok etkenli sistemler arasındaki boşluğu doldurmakta ve analitik çalışmaları gerçekçi ajan dinamikleriyle destekleyen pratik uygulamalarla birleştirmektedir. MATLAB ve ROS ortamlarında gerçekleştirilen simülasyonlar, önerilen metodolojileri doğrulayarak, SVO temelli heterojenliğin sürülerin uyarlanabilirliğini ve performansını artırma potansiyelini ortaya koymaktadır. Bu bulgular, çok etkenli sistemlere kişilik benzeri özelliklerin dahil edilmesi için gelecekteki çalışmalara zemin hazırlamakta ve robotik, otonom araçlar ve karmaşık ortamlarda iş birliğine dayalı görevler gibi uygulamalara dair yeni içgörüler sunmaktadır.

February 2025 **Alp Merzi**

ABSTRACT

Analysis of a Multi-Agent System with Social Value Orientation

The coordination and control of multi-agent systems, including swarms of biological, robotic, or non-physical entities, have been extensively studied over the past three decades. While most research assumes homogeneity among agents, real-world systems are often characterized by behavioral heterogeneity, where agents exhibit diverse interactions and priorities. This dissertation introduces Social Value Orientation (SVO), a psychological concept reflecting individual preferences between self-interest and collective outcomes, as a novel parameter to model and analyze behavioral heterogeneity in swarm systems.

This study investigates the impact of integrating SVO into multi-agent coordination frameworks by examining its effects on swarm dynamics through two applications. The first focuses on a target-capturing task involving quadcopter dynamics, where agents balance individual performance and group cohesion based on their SVO values. Selfish agents prioritize rapid target acquisition, while prosocial agents emphasize swarm cohesiveness, resulting in varied convergence behaviors. The second application explores formation control and rotational behaviors, leveraging SVO to generate grid-like steady-state formations and differential angular velocities. These applications demonstrate how SVO affects spatial arrangements, emergent behaviors, and system performance in diverse scenarios.

This research bridges the gap between theoretical models of social psychology and multi-agent systems also backs up analytical work with practical implementations by employing realistic agent dynamics. Simulations performed in MATLAB and ROS environments validate the proposed methodologies, highlighting the potential of SVO-inspired heterogeneity to enhance swarm adaptability and performance. The findings pave the way for future studies on incorporating personality-like traits into multi-agent systems, offering new insights for applications in robotics, autonomous vehicles, and cooperative tasks in complex environments.

February 2025 **Alp Merzi**

CLAIM FOR ORIGINALITY

Analysis of a Multi-Agent System with Social Value Orientation

This dissertation presents a novel approach to integrating Social Value Orientation (SVO) into multi-agent systems, bridging concepts from social psychology and control theory to explore the effects of behavioral heterogeneity on swarm dynamics. Unlike existing works that predominantly assume homogeneous agent behaviors, this study demonstrates how SVO can be systematically incorporated into coordination mechanisms to influence spatial formations, rotational behaviors, and agent convergence speeds in a structured and predictable manner.

A key contribution of this thesis is the formulation of a method for incorporating SVO into attraction-repulsion dynamics using coordinate coupling matrices, enabling controlled modulation of agent interactions. Analytical validation confirms that steady-state behaviors remain convergent despite the introduction of heterogeneity through SVO. Extensive simulation-based verification further demonstrates that emergent patterns, such as grid-like formations and rotational behaviors, are consistent and repeatable, rather than coincidental. Moreover, this work establishes SVO as a tunable parameter that can be applied to a broad range of multi-agent applications, including robotic swarms and distributed autonomous systems.

By expanding the theoretical foundations of behavioral heterogeneity in multi-agent coordination, this dissertation also introduces practical methodologies that can guide the design of intelligent, adaptive, and decentralized systems. The findings open new research avenues for the hybrid use of SVO and control-theoretic principles, making this dissertation an original and significant contribution to the field.

February 2025 **Alp Merzi**

SYMBOLS

ξ : Social value orientation parameter

a : Acceleration

b_a : Upper bound on the acceleration estimation error

b_v : Upper bound on the velocity estimation error

m : Mass

n : number of agents in a swarm

P : Positive-definite and symmetric matrix

t : Time

u : Control input

v : Velocity

w : Velocity error

x : Position

z : Position error

ABBREVIATIONS

SVO Social Value Orientation. viii

TC-UDAP Target capturing with uncertain data and different agent personalities. viii

UVDAR Ultra violet direction and ranging. viii

LIST OF FIGURES

2.1 Representation of SVO. 16
2.2 The ellipsoidal ring and the specific places where agents must position themselves to solve the TC-UDAP challenge. 20
2.3 quadcopter configuration and body forces. (Figure taken from Toksöz et al. [2019].) 28
2.4 Elliptic distances $z^T Pz$ of the agents to the target. 37
2.5 Trajectories in (x, y, z) of agents with different ξ values. 38
2.6 Trajectories in (x, y) of agents with different ξ values. 39
2.7 The rate at which velocities change in relation to the goal, denoted as $\|w_i(t)\|$. Ultimately, all of them converge to zero, resulting in a static configuration near the objective. There are 10 agents, each with distinct social preferences. The interval $t \in [20, 70]$ is magnified to enhance clarity. 40
2.8 The paths of the agents as they track a target moving in a circular pattern. 42
2.9 Calculate the elliptic distances to the objective for all agents. The agent with a social factor of $\xi_1 = 0.1$ reached the border of the distance zone significantly quicker, at around $t = 20$, compared to the agent with a social factor of $\xi_{10} = 1.0$, who reached the boundary much slower, at approximately $t = 120$. 43
2.10 Visual representations of the agents' positions relative to the goal on a two-dimensional (x, y) plane. 44
2.11 The magnitude of the relative velocities of the agents in relation to the target is denoted as $\|w_i\|$. 45

3.1 Formation of agents based on their team SVO values. Teams with higher SVO values position themselves farther from the center of the swarm. . . 52
3.2 Average distance to the center for each team. As the SVO value increases, the average distance to the center of the swarm increases as well. 53
3.3 Comparison of initial and final average distances of agents to the center. . 55
3.4 Mean squared error of distances between agents and the center. 56
3.5 Range of distances (difference between maximum and minimum distances of agents). 57

3.6 Formation of agents based on their team SVO values. Teams with higher SVO values position themselves farther from the center of the swarm. . . 58
3.7 Average distance to the center for each team. As the SVO value increases, the average distance to the center of the swarm increases as well. 59
3.8 Comparison of initial and final average distances of agents to the center. . 60
3.9 Mean squared error of distances between agents and the center. 61
3.10 Range of distances (difference between maximum and minimum distances of agents). 62
3.11 Superposed Frequency Spectrum for Agent 10 Across All SVO Values (0-15 Hz). The plot shows the variation in frequency components as the SVO value increases, with distinct peaks indicating changes in motion dynamics. 64
3.12 Trajectories of all agents for the first iteration. 65

LIST OF TABLES

2.1 Quadcopter and Controller Parameters 35
2.2 Initial Positions of Agents 36

3.1 Summary of Parameters for Each Scenario 48

1. INTRODUCTION

1.1 Aim of the Study

Multi-agent coordination and control, as well as the consensus, aggregation, and swarming of biological, robotic, or non-physical entities, have been thoroughly investigated over the past three decades. Research on these topics spans diverse disciplines, including control engineering, computer science, biology, and mathematical biology. Significant theoretical advancements have been made in understanding the interactions between agents, while numerous practical applications have emerged. Unmanned ground, aerial, and underwater vehicles, for example, have greatly benefited from these theoretical contributions.

The study of multi-agent coordination and control can be approached at different levels of abstraction. At the foundational level, agents can be modeled with single-integrator dynamics and treated as point-mass entities with no spatial extent. These simple models lay the groundwork for more complex studies, such as those involving the detailed dynamics of quadcopters or autonomous vehicles.

Swarms, by definition, consist of many members, which will be referred to as agents throughout this dissertation. In idealized models, these agents are assumed to be identical in every aspect, including dimensions, dynamics, and internal parameters, forming what is known as a homogeneous swarm. However, in real-world scenarios, perfect homogeneity is rare. Even when physical differences between agents are negligible, behavioral differences may emerge, resulting in heterogeneous behavior. These behavioral variations can give rise to emergent dynamics that, if properly understood and modeled, may offer practical benefits. While much of the literature focuses on homogeneous swarms, the study of heterogeneous agents has recently gained increasing attention. Anisotropic behavior within heterogeneous swarms could hold significant practical value in future research and applications.

The study of multi-agent coordination and control often requires several assumptions, many of which stem from the physical limitations of agents in real-world systems. Consider a case where agents are operating in a three-dimensional environment. To maintain cohesion within the swarm, each agent must be equipped with sensors to detect other agents within its sensing range. These sensors not only help agents avoid collisions but also enable them to position themselves relative to their neighbors.

The concept of neighborhood emerges naturally from the sensing range of an agent. Neighborhood is defined as the set of all agents that lie within a given agent's sensing region. From a graph-theoretical perspective, agents are represented as nodes, and the connections between them are represented as edges. These edges can be bidirectional or unidirectional, indicating whether both agents can sense each other or if only one agent senses the other. If every agent is within the sensing range of all others, the swarm forms a complete graph. If there is a path connecting every agent to every other agent, the swarm is said to be connected.

To mimic natural systems accurately, the study of swarms must adhere to a distributed approach. In such an approach, agents rely only on local information obtained from limited sensors. This means that each agent has access only to information from nearby neighbors within its sensing region. This distributed nature raises significant challenges related to connectivity and sensing regions. Even for swarms governed by the simplest dynamics, connectivity plays a crucial role in ensuring group cohesion and consensus. However, the focus of this dissertation is not on connectivity issues. Instead, we assume that the interaction topology of the swarm is either connected or complete and direct our attention to the behavioral heterogeneity of agents.

Social Value Orientation (SVO) is a concept from social psychology that reflects an individual's stable preference regarding the allocation of resources between themselves and others. SVO serves as an indicator of the extent to which an individual prioritizes personal outcomes over collective or social outcomes. It is a fundamental construct used to explain human behavior in social dilemmas, cooperative activities, and competitive environments, providing insight into how individuals balance self-interest with social concern.

SVO examines the motivations underlying social interactions by analyzing how individuals behave when making decisions that affect both their own welfare and that of others. Individuals can be classified into distinct categories based on their value orientation.

Prosocial Orientation: Individuals prioritize fairness and equality, seeking to maximize joint outcomes for both themselves and others. They favor cooperative solutions that ensure mutual benefit.

Individualistic Orientation: Individuals focus solely on maximizing their own outcomes, regardless of the impact on others. Their behavior is driven by personal gain, with little regard for social equity.

Competitive Orientation: Individuals strive to maximize their relative advantage over others, even if it comes at the expense of reducing overall outcomes. Their actions foster rivalry by seeking better results than others.

In this thesis, the core concept of SVO is applied to multi-agent systems to introduce behavioral heterogeneity within the swarm. We interpret swarm cohesiveness as the collective outcome of the group and the achievement of individual goals (such as reaching a target) as the personal outcome of each agent. By varying the SVO parameter, we create a spectrum of agent behaviors ranging from highly prosocial to highly competitive.

The behavioral differences introduced through SVO result in meaningful steady-state variations among the agents. As agents move from one end of the SVO spectrum to the other, the emergent behavior changes accordingly. For example, agents with higher SVO values exhibit stronger cooperative tendencies, while those with lower SVO values act more selfishly. These behavioral differences influence the overall formation and cohesiveness of the swarm, highlighting the importance of heterogeneity in achieving diverse system objectives.

This dissertation focuses on the impact of behavioral heterogeneity on swarm dynamics, with a particular emphasis on the role of SVO. While much of the existing literature assumes homogeneity among agents, we investigate how introducing behavioral differences through varying SVO values affects the swarm's spatial distribution and steady-state behavior. Additionally, we examine how these differences influence the ability of agents to coordinate and maintain group cohesion in dynamic environments.

1.2 Overview of the Study

This dissertation is composed of two distinct chapters. Chronologically, the first chapter applies SVO to agents governed by full quadcopter dynamics. In this scenario, the agents

solve a target-capturing problem within an ellipsoidal region. The results demonstrate that agents with higher selfishness prioritize reaching the target more aggressively, while those with a more prosocial orientation focus on maintaining the group's cohesiveness. The second chapter introduces SVO as a parameter in the attraction-repulsion functions to generate varied steady-state formations and rotational behaviors in a simulation-based scenario.

Although these two cases address different problems—one being a target-capturing task and the other a formation control problem with rotational behavior—both integrate SVO as a core parameter. The outcomes of these investigations highlight the potential for behavioral heterogeneity in swarms, with SVO serving as a practical means to achieve it. These findings suggest that behavioral heterogeneity, inspired by concepts like SVO, may have broad applications in future multi-agent systems.

In the first scenario, the study builds upon prior work that addressed the target-capturing problem for a group of agents modeled as double integrators. In this setup, each agent has access to the relative location of the target and only approximates its velocity and acceleration. Given that the estimation errors are bounded, a control law was designed to ensure that all agents would converge within an ellipsoidal region around the target, which serves as the goal.

Additionally, each agent possesses local knowledge of its neighbors within a defined sensing range. We incorporated SVO as a parameter into the control law to modify the agents' attractive forces. The results indicate that the revised control law maintains its original convergence guarantees, guiding agents toward the predefined circular or ellipsoidal region surrounding the stationary target. The introduction of SVO, however, causes agents to exhibit distinct behaviors based on their assigned SVO values. Selfish agents converge more quickly to the steady state, while prosocial agents interact more extensively with the swarm, fostering greater cohesion but at the cost of slower convergence.

This part of the study demonstrates that behavioral heterogeneity through SVO leads to diverse steady-state behaviors within the swarm. These differences reflect varying priorities: selfish agents prioritize reaching the target faster, while prosocial agents aim to balance individual goals with maintaining group cohesion.

The second chapter focuses on using SVO to create grid-like steady-state formations and varying rotational velocities. This scenario is inspired by literature that employs

coordinate-coupling matrices to achieve swarm formations with rotational behaviors. We extended this framework by integrating SVO into the coordinate-coupling matrices, altering the agents' steady-state configurations and their angular velocities during rotational motion.

The simulation results reveal that SVO influences the agents' behavior in two key ways. First, different SVO values can generate a grid-like pattern at steady state, where agents with similar SVO values form concentric layers based on their behavioral priorities. Second, SVO affects the rotational velocities of the agents, with selfish agents displaying faster angular velocities compared to their prosocial counterparts. These results highlight how SVO can shape both the spatial arrangement and the dynamic behavior of multi-agent systems.

The original contribution of this dissertation lies in the novel integration of SVO into the coordination of multi-agent systems. This study demonstrates that behavioral heterogeneity can be modeled as a form of personality variation within swarms, where agents exhibit behaviors ranging from selfish to altruistic or asocial to highly cooperative.

Our analysis shows that SVO can be seamlessly incorporated into existing control laws without compromising convergence properties. We further demonstrate that SVO can be employed in novel ways to generate different rotational behaviors and steady-state formations. These findings open new avenues for the application of heterogeneous personalities in multi-agent systems, suggesting that agents with diverse behavioral traits can enhance performance in various scenarios.

In summary, this dissertation explores the integration of SVO into multi-agent systems, examining its effects through two distinct applications. The first application involves a target-capturing task using quadcopter dynamics, where SVO influences the trade-off between individual performance and group cohesion. The second application investigates the use of SVO to create varied steady-state formations and rotational behaviors. Through these studies, we demonstrate that SVO-inspired behavioral heterogeneity has significant potential for improving the performance of multi-agent systems and providing new insights for future research.

1.3 Literature Review

The literature review of this dissertation is the collective of three parts. The first part focuses on the literature related to the foundational frameworks upon which this study builds. Those frameworks include the cases in chapters 2 and 3, the models that have been used in those chapters, the theoretical background of those cases, as well as the framework needed for the simulations. The second part explores research on SVO, which serves as a key inspiration for the creative aspects of this work. The third part examines heterogeneous behavior in multi-agent systems, providing the necessary context for situating this study within the broader body of research.

The field of multi-agent systems, particularly the coordination of Unmanned Aerial Vehicles (UAVs) and UAV swarms, has garnered significant attention over the past decade. The collective behavior of swarm systems Gazi and Passino [2011] is not only a compelling natural phenomenon but also holds vast potential for engineering applications, including search and rescue operations, surveillance and reconnaissance, exploration, and defense. One of the key challenges within these applications is the problem of target tracking and capturing Sepulchre et al. [2006], which is the case in chapter 2. It involves surrounding or enclosing a specific target using local information from individual agents within the swarm. Hunting whales is a classic example of target capturing in nature Goldbogen et al. [2013], Merzi and Gazi [2017].

An important feature of distributed swarm algorithms, particularly in the target capturing problem, is achieving the objective with limited sensing abilities and local information Kim and Sugie [2007], Kobayashi et al. [2006]. These constraints introduce several challenges; for instance, agents might only possess incomplete or imprecise information about the target. Moreover, if the target is moving, agents may not have accurate data on its motion. Nonetheless, many studies in the literature assume that perfect information about the target is available.

The ability of multiple vehicles to monitor a given state trajectory, often referred to as consensus or coordinated tracking, was initially explored within the field of multi-agent control Ren [2008]. More recent research, however, has primarily concentrated on confinement control. In this approach, followers are assumed to operate within a convex region defined by several leaders, whose behavior is theoretically modeled Cao et al. [2010], Wang [2016].

These studies are driven by a variety of applications, such as teams of heterogeneous vehicles navigating between different goals while relying on information provided by a small subset of vehicles, all within obstacle-filled environments. Containment control methods, as outlined in Ji et al. [2008], Li et al. [2011], Lou and Hong [2012], Zheng and Wang [2014], Liu et al. [2020] and related works, are fundamentally consensus-based algorithms. A more complex operational scenario arises when an additional, non-trivial geometric constraint is introduced to the containment control problem: all vehicles must remain within a non-convex region (referred to as the capturing region). This region is defined as the area between the containment region and an inner prohibited zone (known as the distancing region).

Potential function methods have been extensively employed to design swarm coordination strategies, including for target capturing tasks. These methods utilize mathematical functions that encode attractive or repulsive forces among agents, ensuring the swarm maintains cohesion while avoiding collisions. In Blázovics et al. [2012] and Kobayashi et al. [2006], for example, potential functions are used to enable agents to surround a target in a 2D space using decentralized control methods. Yao et al. [2007] further enhances this approach by considering fully actuated agents with model uncertainties and integrating sliding mode control strategies to ensure the agents successfully capture a moving target. Additionally, Halcı et al. [2019] extends these results to non-holonomic agents, demonstrating the general applicability of potential function-based approaches across different agent types and dynamics.

Another well-known strategy in multi-agent coordination is cyclic pursuit, where agents follow predefined trajectories in pursuit of a target. In Kim and Sugie [2007], Lin et al. [2004], and Marshall [2005], this method is studied in planar environments, demonstrating the feasibility of target capturing through cyclic pursuit. The work in Kim and Sugie [2007] further extends this concept to 3D spaces, showcasing the adaptability of the approach across different spatial dimensions. However, one of the primary limitations of these approaches is the assumption that agents have access to perfect information about the target, an assumption that may not hold in practical scenarios.

Many studies assume simplistic agent dynamics, such as single or double integrators, which may not fully capture the complexities of real-world UAV systems. In real-world scenarios, the agents in a swarm often operate with imperfect information regarding the target. This uncertainty complicates the problem of capturing a target, especially when

the agents can only estimate certain properties of the target, such as its velocity and acceleration. For instance, the work presented in Bono et al. [2022] develops a target capturing strategy for swarms of double integrator agents, accounting for uncertainties in the target's motion. Furthermore, perfect information assumptions about the target's position, velocity, and acceleration often oversimplify the problem. In practical applications, however, sensing errors and communication disruptions are inevitable. The current study addresses these challenges by implementing quadrotor dynamics Mellinger et al. [2012],Toksöz et al. [2019], Merzi et al. [2022]. This extension bridges the gap between theoretical frameworks and practical implementations, contributing to the development of more robust multi-agent coordination strategies. Furthermore we employed Ultra-Violet Direction And Ranging (UVDAR) Walter [2019], Walter et al. [2019] technology, which enables relative self-localization without relying on GPS data. This approach allows for local interactions between agents, fostering decentralized behavior within the UAV swarm. This addresses the oversimplification issue that stems from assuming perfect information.

Advancements in sensing, processing, and communication technologies have enabled the development of more advanced UAV systems and realistic implementations of swarm algorithms. The availability of technologies such as UVDAR has facilitated the deployment of UAV swarms with decentralized control architectures, where individual agents rely only on local information. In this study, simulations in chapter 2 are performed using both MATLAB and Robot Operating System (ROS) environments to verify the feasibility of the proposed control strategies. For ROS simulations we benefited from the framework developed at CTU Baca et al. [2021]. The target-capturing task is modeled as convergence to an ellipsoidal region centered on the target, with both an inner and outer boundary that defines the valid operating region for the agents.

The use of non-convex regions, such as the ellipsoidal ring employed in Chapter 2, poses unique challenges for swarm coordination. The control framework adopted here ensures that all agents, regardless of their individual SVO values, converge to the desired region. This work demonstrates that SVO not only affects the convergence speed but also influences the agents' steady-state behavior, paving the way for future research into personalized agent dynamics within heterogeneous swarms.

In Chapter 3, the model presented in Fedele et al. [2022] was adopted and extended. This paper builds on the original Gazi–Passino swarm model Gazi and Passino [2004] by incorporating Cartesian coordinate-coupling matrices, enabling the simulation of more complex

swarm behaviors, including rotational motion. While the original Gazi–Passino model focused primarily on stability, aggregation, and cohesion through attraction-repulsion functions, it did not address rotational dynamics.

The primary innovation of the extended model lies in the use of two matrices to couple agent coordinates, offering greater flexibility in agent interactions. Through the adjustment of these matrices, the swarm can transition between static configurations, dynamic formations, or rotational behaviors around a defined centroid.

This model serves as the foundation for the second case study in the current dissertation, which explores how varying SVO parameters affect swarm behaviors, including steady-state patterns and angular velocities. Through this integration, we aim to demonstrate how heterogeneity within the swarm can influence both spatial arrangements and dynamic movement patterns.

The literature presents various applications of SVO in multi-agent systems, robotics, and autonomous vehicles. For instance, Pierson et al. [2020a] applies SVO concepts to collision avoidance by incorporating SVO weights into Voronoi tessellations, where agents with higher SVO values are assigned larger Voronoi regions. In Schwarting et al. [2019], SVO is used to predict human driver behavior and optimize autonomous vehicle trajectories, while Buckman et al. [2019] uses it for traffic flow optimization at intersections. However, these applications generally involve competitive environments, where agents or actors pursue different or conflicting objectives.

In contrast, the application of SVO in this dissertation focuses on cooperative swarm behavior, where all agents share the same goal of target capturing or enclosing a target region. We extend the use of SVO beyond competitive environments to demonstrate its potential in non-competitive, collaborative settings. Specifically, in our study, SVO affects the agents' interaction terms within the swarm and their approach toward the target. Selfish agents (with low SVO values) prioritize target tracking, engaging less with other agents and converging rapidly toward the target. Conversely, social agents (with high SVO values) prioritize maintaining cohesion with the swarm, leading to more interaction with neighboring agents but a slower convergence to the target. This interplay between individual goals and group cohesion highlights the flexibility and utility of SVO in designing heterogeneous multi-agent systems.

The use of SVO to generate behavioral heterogeneity in swarms opens up new possibilities

for swarm coordination research. Most prior studies on multi-agent coordination have focused on homogeneous agents, assuming identical dynamics and behaviors. However, as the research on heterogeneous swarms evolves, it becomes evident that introducing behavioral diversity through parameters like SVO can lead to emergent behaviors that have practical applications. For instance, anisotropic behavior stemming from differences in SVO values may enhance swarm adaptability in dynamic environments.

Heterogeneity of swarms is mostly studied under anisotropic swarms. One of the early works on the subject is Chu et al. [2003]. Author introduces an extension to the isotropic swarm model developed in Gazi and Passino [2004]. The primary goal is to analyze how anisotropic interactions among swarm agents affect their collective behavior, cohesion, and stability. The model uses attraction-repulsion dynamics to simulate swarm behavior, with anisotropic interactions allowing the interaction strength between agents to vary. Unlike isotropic models, where interactions are uniform, the anisotropic model accounts for variations based on the relative positions or other factors between agents. The core idea is that swarms exhibit self-organized motion and form cohesive clusters, despite heterogeneity in interaction patterns. The paper rigorously proves that the swarm remains cohesive and aggregates around a stationary center, leveraging concepts from potential fields and Lyapunov stability analysis. Notably, the swarm's center of mass remains stationary under anisotropic interactions, even though individual agents continue to move relative to it. Through mathematical analysis, the authors demonstrate that anisotropic swarms can achieve complete stability, meaning all agents converge to equilibrium points over time.

Afterwards, in Chu et al. [2006] explores the collective behavior of anisotropic swarm models, once more extending the classical isotropic swarm model presented in Gazi and Passino [2004] by introducing differing interaction strengths among pairs of agents. This more general approach aims to reflect realistic scenarios where agents may interact with varying strengths due to differences in their characteristics or communication capabilities.

The authors investigate two types of swarm systems: reciprocal and non-reciprocal swarms. In reciprocal swarms, interactions between two agents are symmetric (i.e., they affect both agents equally). For such swarms, the authors prove that the center of the swarm remains stationary over time and that the system achieves complete stability. They also show that agents will aggregate and form a cohesive cluster around the stationary swarm center. The behavior of reciprocal swarms is strongly influenced by the eigenstructure of the connection matrix, which provides deeper insights into how interaction

patterns affect swarm dynamics.

In contrast, non-reciprocal swarms —where interactions between agents are asymmetric— exhibit more complex dynamics. While these systems no longer maintain a stationary center, they can still achieve aggregation under specific conditions known as the detailed balance condition. The paper provides analytical results demonstrating that non-reciprocal swarms may still achieve stability, though their dynamics are more intricate. The most interesting finding in the non-reciprocal case is the emergence of oscillatory behavior, which is purely self-organized and not driven by any external forces. This oscillatory motion highlights the importance of interaction asymmetry in generating complex emergent behaviors.

Heterogeneity has not only been studied within the scope of non-reciprocity due to interaction strengths. In Zheng and Wang [2012] authors addresses the consensus problem in multi-agent systems consisting of both first-order and second-order agents. The paper focuses on how agents with heterogeneous dynamics (different integrators) achieve consensus when interacting within fixed or switching topologies. The paper explores the coordination challenges in heterogeneous multi-agent systems, where agents follow either first-order or second-order dynamics. It proposes two consensus protocols tailored for each type of agent. The theoretical framework is grounded in graph theory and nonnegative matrix theory, which help establish necessary and sufficient conditions for consensus with fixed topology. The study also derives sufficient conditions for systems with switching topologies, which present additional complexity. A significant challenge addressed in the paper is that heterogeneous systems, unlike homogeneous systems, cannot directly apply Laplacian matrix diagonalization techniques. Therefore, the authors provide alternative conditions ensuring consensus through directed spanning trees, a critical requirement for ensuring coordinated behavior.

Heterogeneity of swarms are also studied from the perspective of other disciplines such as Zoology. In Kengyel et al. [2015] authors explore the advantages of behavioral heterogeneity in swarms through a case study inspired by juvenile honeybees. It investigates the hypothesis that swarms with heterogeneous behaviors —agents having distinct, static roles— can outperform homogeneous swarms in aggregation tasks. The research draws inspiration from honeybees, which display task specialization and limited task switching based on age. In this study, four predefined behavior types are modeled: random walkers, wall followers, goal finders, and immobile agents, mimicking the behaviors observed in

honeybees.

The paper presents a mathematical model to describe these behavior types and uses evolutionary algorithms to determine optimal compositions of behavior types for various tasks. Through simulations, the authors examine two scenarios: aggregation around a single goal area and a choice between two goal areas. The results show that heterogeneous swarms, optimized through evolutionary algorithms, consistently outperform homogeneous swarms in both tasks.

The study's findings highlight that behavioral diversity enhances the swarm's adaptability and performance by fostering cooperation between agents with different strategies. These results suggest that swarm systems designed with predetermined, heterogeneous behaviors —rather than dynamic task switching— can offer practical advantages. The authors argue that these insights can be extended to the field of swarm robotics and applied in future engineering solutions.

The work Pierson et al. [2020b] in 2020, introduces the concept of Weighted Buffered Voronoi Cells (WBVC) to model distributed, semi-cooperative behavior in multi-agent systems. By integrating SVO into Voronoi tessellation, the authors encode varying degrees of social preferences—ranging from egoistic to altruistic—directly into the navigation policies of the agents. The WBVC framework ensures collision-free maneuvers, with agents navigating within their Voronoi cells while maintaining a safety buffer between boundaries. Not explicitly noted in the paper, this can be seen as a form of heterogeneity among swarm members. The novel contribution of this study lies in weighting the Voronoi cells asymmetrically based on agents' SVO, where more selfish agents have larger Voronoi regions, giving them a strategic advantage in terms of maneuverability. Altruistic agents, with smaller Voronoi regions, are more likely to yield to their selfish counterparts. This method allows the authors to model semi-cooperative systems where cooperation is not uniformly distributed among agents.

One of the most comprehensive surveys on heterogeneus swarms was conducted in 2022 Bao et al. [2022]. The survey emphasizes how heterogeneity in multi-agent systems where they use the abbreviation (MASs) introduces new complexities compared to homogeneous systems and explores how cooperative control strategies can address these challenges. Heterogeneity can be broadly classified into two types: weak heterogeneity

and strong heterogeneity. Weak heterogeneity refers to systems where agents follow similar dynamic structures, such as identical differential equations, but differ in their parameters, such as mass, speed limits, or inertia. An example would be a swarm of UAVs with varying speeds or capacities. From that classification perspective studies in this dissertation falls into the weak heterogeneity category, since SVO is added into control equations with a varying parameter. Strong heterogeneity, on the other hand, involves agents with fundamentally different dynamics, such as aerial and ground vehicles working together in a collaborative task, resulting in distinct control models for each type of agent. This anisotropic behavior, resulting from physical or behavioral differences, introduces significant complexity into the coordination and control of the swarm.

The survey discusses several cooperative control strategies designed to manage heterogeneity, focusing on achieving consensus, formation, and containment. Consensus control ensures that all agents converge to a shared state, such as velocity or position, despite their differences. Techniques such as observer-based and adaptive control help agents estimate and adjust to each other's behaviors. Formation control aims to arrange agents into specific patterns, maintaining desired configurations like grids or circles. This study shares similar aims since in chapter 3 grid-like configuration is achieved. Event-triggered control strategies reduce resource consumption by allowing agents to communicate only when necessary to maintain formation. Containment control involves leader-follower dynamics, where leader agents converge to a specific region, and follower agents subsequently align with them.

Handling switching topologies, where communication links between agents change dynamically, is another key challenge for heterogeneous systems, where we have not particularly addressed in our dissertation. The survey highlights the use of Markov switching systems and time-varying graph models to manage these dynamic interactions. These approaches enable agents to maintain coordination even when communication is intermittent or the agents are moving. Additionally, the growing complexity of heterogeneous systems has necessitated the development of fault-tolerant control mechanisms, ensuring that the system remains operational even if individual agents fail. Secure control strategies are also essential to protect against cyber-attacks, such as jamming or spoofing, which can disrupt coordination, especially in heterogeneous systems with varied agent capabilities.

The survey identifies several open research areas, such as extending cooperative control

to systems with higher-order dynamics and developing methods for discrete-time heterogeneous systems. Additionally, network-induced constraints, including time delays and packet losses, remain significant challenges for heterogeneous systems, calling for further research on event-triggered mechanisms to address these issues.

This survey provides a comprehensive overview of the challenges and strategies involved in managing heterogeneous multi-agent systems and offers insights into how behavioral heterogeneity can enhance system performance. In the light of this overview, the relevance of these findings to this dissertation lies in the potential for SVO to introduce a new dimension of behavioral heterogeneity within swarms. By applying SVO, behavioral differences among agents can be leveraged to create varying swarm formations and improve coordination. This integration aligns with the broader research direction highlighted in the survey, emphasizing the practical applications of heterogeneity in multi-agent systems.

2. APPLICATION OF SVO TO A TARGET CAPTURING PROBLEM

This chapter examines the process of target capturing by a group of agents exhibiting varying levels of social behavior, ranging from self-interested to highly social. To achieve this, we used a parameter to quantify SVO, a concept from social psychology that measures an individual's degree of sociability Liebrand [1984]. In social dilemmas, individuals may prioritize their own benefits to different extents compared to those of others, with this prioritization level quantified by the SVO. We incorporated the SVO structure directly into our control method through a dedicated parameter. Although the following chapter explore various methods for integrating SVO in multi-agent systems, other potential approaches could be effective as well; however, these are beyond the scope of this thesis.

By including SVO as a controller parameter, it becomes possible to assign unique personalities and roles to agents. This is achieved despite the fact that all agents utilize the same control algorithm. As a result, they are able to work together harmoniously to accomplish a shared objective. The control algorithm we have developed consists of several terms, each serving distinct objectives. More precisely, it encompasses terminology related to the collective behavior of a group, such as how they interact with one other, their tendency to be drawn towards or pushed away from a specific target, and their ability to estimate the speed and change in speed of an unknown target. An agent with asocial tendencies, indicated by a low SVO weight in the control protocol, may have reduced interaction with the swarm and prioritize quickly approaching the objective. On the other hand, an altruistic(selfless, social) agent that has a larger SVO parameter engages stronger interactions with other agents. It tries to ensure collision avoidance with anyone else in the swarm also moves towards the designated area. The variation in agent behavior leads to a more flexible and responsive approach to accomplishing the job within the group. Furthermore, our approach guarantees that every agent may efficiently contribute to the shared objective,

regardless of their various levels of social engagement.

Various methods can be used to represent SVO. One approach is to use the angular representation Pierson et al. [2020a], Liebrand [1984], Murphy et al. [2011], this visualization is illustrated in Figure 2.1. Another method is to represent SVO with a linear weight $\xi \in (0, 1]$. This is derived from the angle ϕ using the formula $\xi = \frac{2\phi}{\pi}$. By assigning different ξ values to agents, where $\xi_i \approx 0.1$ denotes selfish, $\xi_i \approx 0.5$ denotes moderate, and $\xi_i \approx 1$ denotes altruistic characteristics, agents can be differentiated. This thesis adopts this approach.

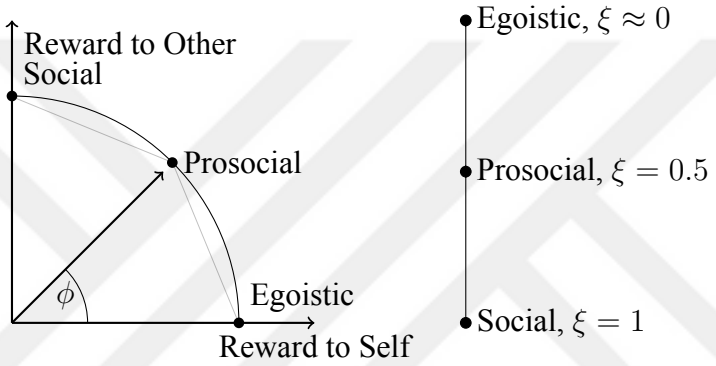

Figure 2.1: Representation of SVO.

In our study, we incorporate ξ_i into the control protocol, where it has a proportional impact on the interaction between individuals in the swarm and an inverse effect on the target tracking term.

The subsequent portion of this chapter is structured in the following manner: Section 2.1 provides a clear formulation of the target capturing problem for a swarm of double integrator agents with diverse personalities. It also presents a proof that despite their various social preferences, the agents will effectively capture or enclose the target. Section 2.2 provides a comprehensive explanation of the quadcopter model and how it is combined with the control protocol. Section 2.3 showcases the simulation results acquired using Matlab, demonstrating the impact of the agents' social preferences on quadcopter dynamics.

2.1 Problem Definiton

This part will provide a concise overview of the problem formulation discussed in Bono et al. [2022], as well as the recently added social preference (i.e., character or personality) to the swarm members. To achieve this goal, let us examine a group of agents that have no physical dimensions. Let's consider a swarm composed of n agents. The agents' movements occur in a Euclidean space with $d \geq 2$ dimensions. The dynamics of the agents may be described as a double integrator, which means they behave as point masses.

$$\begin{aligned} \dot{x}_i(t) &= v_i(t), \\ \dot{v}_i(t) &= \frac{1}{m_i} u_i(t), \quad i = 1, 2, 3, \ldots, n. \end{aligned} \tag{2.1}$$

In Equation (2.1), $m_i > 0$, $x_i(t) \in \mathbb{R}^d$, and $v_i(t) \in \mathbb{R}^d$ denote the positive mass, position, and velocity of the i'th agent at time $t \geq 0$, respectively. The control input, represented as $u_i(t) \in \mathbb{R}^d$, refers to the force exerted to facilitate the movement of the agents. The point mass dynamics described in (2.1) is a widely used agent model in research for developing proof-of-concept results. Once results are obtained for agents with specific dynamics, they can be easily adapted to fit those dynamics. That's the approach we employ in this chapter. Firstly, we establish the findings specifically for agents with double integrators, and subsequently, we illustrate how these findings may be modified and applied to agents with quadcopters.

The goal is for the agents, regardless of whether they are social or asocial, to locate and apprehend a target that is either stationary or in motion. The target's location state and velocity state when time is equal to t are represented by $x_T(t)$ and $v_T(t) = \dot{x}_T(t)$, accordingly. We make the assumption that $x_T(t)$ belongs to the class $\mathcal{C}^2$. The differences between states for agent i in relation to the desired states have been defined by

$$\begin{aligned} w_i(t) &= v_i(t) - v_T(t) \\ z_i(t) &= x_i(t) - x_T(t), \quad i = 1, 2, \ldots, n. \end{aligned} \tag{2.2}$$

Then, the dynamics for the i'th agents errors become

$$\begin{aligned} w_i(t) &= \dot{z}_i(t) \\ \frac{1}{m_i} u_i(t) - a_T(t) &= \dot{w}_i(t), \quad i = 1, 2, 3, \ldots, n, \end{aligned} \tag{2.3}$$

$a_T(t)$ is used for the first derivative of the velocity of the desired state. That vector is an element of d dimensional real numbers. The target's dynamics, including the path it takes $\{x_T(t), \dot{x}_T(t), \ddot{x}_T(t)\} = \{x_T(t), v_T(t), a_T(t)\}$, are presumed to be deterministic but remain unknown. Put simply, the target movement excludes any random factors. However, the inclusion of stochasticity within the existing framework is not explored in this context. The most basic situation involves considering the target being a point mass agent, although this method can also be applied to targets that are not point masses.

The entire group is assumed to possess sensors capable of measuring the actual location $x_T(t)$ of the target. However, the agents do not have access to data regarding the target's velocity positions first and second derivatives ($v_T(t)$,$a_T(t)$). Hence, the agent employs calculations of those values (which can be determined using any appropriate method) and represents these calculations as $\hat{v}_T^i(t), \hat{a}_T^i(t) \in \mathcal{C}^0$. Additionally, we use the assumption that the errors in sensing on these estimations are limited and have predetermined boundaries:

$$\begin{aligned} b_v &> \left\| -\hat{v}_T^i(t) + v_T(t) \right\|, \\ b_a &> \left\| -\hat{a}_T^i(t) + a_T(t) \right\|, \end{aligned} \tag{2.4}$$

The primary source of uncertainty in this scenario stems from the unknown nature of the target's dynamics, resulting in its velocity as well as acceleration being predicted with potential errors based on position measurements. The estimations are continuous, and the related estimation errors are limited. This configuration is highly authentic and frequently found in swarm robotics applications. An example of determining the target's relative position is by use a sensor like UVDAR Walter et al. [2019]. The UVDAR system is a sensing technology that functions in the ultraviolet (UV) band. It provides precise measurements of relative position and yaw, regardless of ambient circumstances and the movement of the object. Afterwards, the velocity and acceleration of the target can be approximated using a suitable technique.

As the agents maneuver towards the target with the objective of capturing or enclosing it, they must also ensure a safe distance from the target and from each other. This requirement arises due to the need to avoid collisions or for other practical considerations that may vary depending on the application scenario.In order to ensure this margin, we establish a specific area called the distancing region, where individuals must maintain safe distances from each other. The designated area where individuals are allowed to gather is known as the containment region. The shape of these regions is defined by the matrix P. This is a positive-definite and a symmetric matrix. The matrix's properties, such as its eigenvalues and eigenvectors, dictate whether the region takes the form of an ellipse or a circle. The area where agents arrange themselves around the target is the middle portion, which is shaped like an ellipse and located between the outer border (which defines the containment region) and the inner boundary (which defines the distancing region). Regardless of their preferences, agents should remain within this ellipsoidal ring. This can be seen in Figure 2.2 for a 2-D space, specifically for $\mathbb{R}^2$.

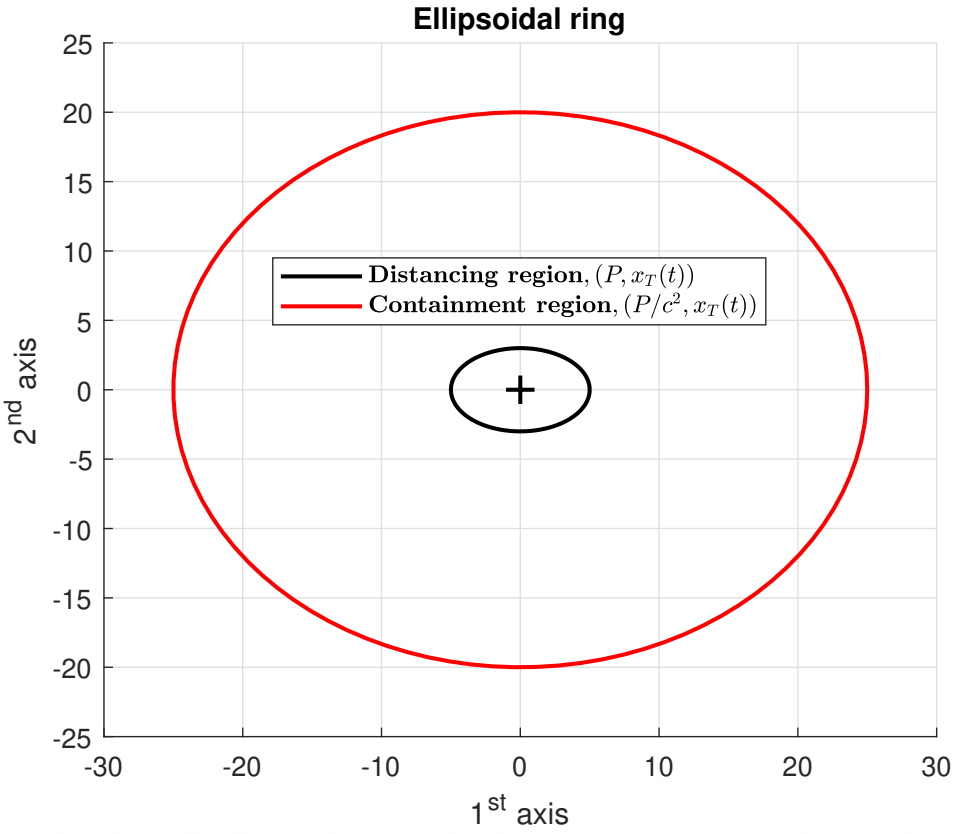

Figure 2.2: The ellipsoidal ring and the specific places where agents must position themselves to solve the TC-UDAP challenge.

Below, we formally define the problem.

Problem: Target Capturing with Uncertain Data and Different Agent Personalities (TC-UDAP). Consider a situation in which we have information about the location of a target, but we are unsure about its speed and rate of change of speed. A swarm with n members, all of them with exact dynamics as defined in (2.3), intends to capture the target. Each agent has distinct SVO parameters, which indicate diverse social preferences or personalities. These parameters are denoted by $\xi_i \in (0, 1]$ for $i = 1, 2, \ldots, n$. Given the SVO parameters ξ_i and the positive definite symmetric shaping matrix $P = P^\top > 0 \in \mathbb{R}^{d\times d}$, the objective is to calculate the control inputs $u_i(t) \in \mathbb{R}^d$ for each agent $i = 1, 2, \ldots, n$, in order to fulfill the following conditions:

- Distancing: The ellipsoid defined by $\mathcal{E}\left(P, x_T(t)\right)$ must not be breached by any agent in the swarm. Formally, for all $i = 1, 2, \ldots, n$ and for all $t > t_0$, if $x_i\left(t_0\right) \notin$

$\mathcal{E}\left(P, x_T\left(t_0\right)\right)$, then $x_i(t) \notin \mathcal{E}\left(P, x_T(t)\right)$.

- Containment: The containment region is defined by the ellipsoid $\mathcal{E}\left(P/c^2, x_T(t)\right)$, where the swarm is required to converge. The parameter c scales this region, and it is influenced by the uncertainties in the target's velocity and acceleration. Specifically, there exists a limit $\underline{c}\left(b_v, b_a\right) \geq 1$ such that, at steady-state, the agents satisfy $x_i(t) \in \mathcal{E}\left(P/c^2, x_T(t)\right)$ with $c > \underline{c}\left(b_v, b_a\right)$ for all $i = 1, 2, \ldots, n$.

For a change from the control algorithm outlined in Bono et al. [2022], we incorporate the SVO component ξ_i into our controller to allow for varied behavior among the agents.

$$\begin{aligned} u_i(t) =& \frac{1}{\xi_i}\left(-\alpha_i P z_i(t) + \frac{P z_i(t)}{z_i(t)^\top P z_i(t) - 1}\right) \\ & - \gamma\left(v_i(t) - \hat{v}_T^i(t)\right) + m_i \hat{a}_T^i(t) + \xi_i \beta_i h_i(t), \end{aligned} \tag{2.5}$$

The variable ξ_i symbolizes the social value of the agent i, where ξ_i is a value between 0 and 1 (excluding 0 and including 1). The parameters α_i, β_i, and γ are controller parameters, and they are all positive real numbers.

The initial term in the control rule, with $\alpha_i > 0$ serving as an attraction parameter, guarantees that the agent is pulled towards the destination. Conversely, the second term prohibits the agent from getting into the region of distancing.

The third term corresponds to a velocity alignment factor having a positive coefficient γ, which takes into account the predicted velocity. The fourth term serves as a feedforward element to estimate the target acceleration. The term $h_i(t)$ is a function that expresses the interaction between members of a swarm. It is defined as

$$h_i(t) = \sum_{j \in \mathcal{N}_i(t)} g\left(\left\|\xi_i z_i(t) - \xi_j z_j(t)\right\|\right)\left(\xi_i z_i(t) - \xi_j z_j(t)\right) \tag{2.6}$$

The notation $\mathcal{N}_i(t)$ represents the collection of neighboring agents of agent i at time t. This term, characterized by a repulsion coefficient $\beta_i > 0$, is employed for the purpose of avoiding collisions, while simultaneously having the capability to include attraction among agents. The impact of it is directly related to the SVO value ξ_i.

The function $g \in \mathcal{C}^0 : \mathbb{R}^+ \to \mathbb{R}$ in (2.6) has properties as below:

$$\sigma < g(\|y\|)\|y\|, \quad \text{for all y,} \tag{2.7}$$

However, if $||y||$ is greater than the sensing range of the agents (r_v) then $g(\|y\|)y = 0_d$. This is valid for some $\sigma > 0$ and $r_v > 0$. These conditions imply that the inter-agent repulsive force is bounded by the parameter σ, becomes zero at a certain distance r_v, and remains zero for any distances greater than r_v. Essentially, r_v represents the range within which agents sense and repel each other, or, more fundamentally, the effective range of their proximity sensors.

2.1.1 Analysis of the Target Capturing with Uncertain Data and Varying Personalities Problem

The analysis of swarm behavior with various agent characteristics, as described in the TC-UDAP Problem, employs an approach akin to the analysis published in Bono et al. [2022]. Nevertheless, certain distinctions emerge as a result of integrating the SVO element within the control method. Prior to presenting the study of the agents' behaviors and the proposed solution to the TC-UDAP we present a lemma from Bono et al. [2022]. This lemma is going to be utilized in the proof of our findings.

Lemma 1. (Bono et al. [2022]) Let $f(y) = p + py - \log(y)$ with $p \in \mathbb{R}$, and $y \in \mathbb{R}^+$. If $p > W_0(1/e)$, where $W_0(\cdot)$ is the principal branch of the Lambert W function, then $f(y) > 0$ holds.

To find solid proof supporting this lemma and obtain additional information, one can consult the reference Bono et al. [2022]. The accompanying analysis use the result of this lemma. Using this outcome, we will prove that the speeds of the agents stay within a certain range under the control method specified in equation (2.5), when the SVO parameter is taken into account. First, we show that swarm members velocities are bounded with respect to the target.

Lemma 2. Consider the swarm described by the model (2.3). Assume that the control law in (2.5) is applied to all agents with the condition

$$\alpha_i > W_0(1/e)$$

being satisfied. Then, for all agents, the velocity errors $w_i(t), i = 1, 2, \ldots, n$, are ultimately bounded by

$$\|w_i(t)\| \leq \overline{w}_i = b_v + \frac{\xi_i \beta_i n\sigma + m_i b_a}{\gamma}. \tag{2.8}$$

Proof. Consider the Lyapunov function

$$V_{i1} = \frac{1}{2}\left(\frac{\alpha_i}{\xi_i} z_i^T P z_i - \frac{\ln(z_i^T P z_i - 1)}{\xi_i} + m_i w_i^T w_i\right) \tag{2.9}$$

where α_i is larger than $W_0(1/e)$. In this case, V_{i1} is consistently positive. This is because the sum of the first two terms is positive, as stated in Lemma 1, and the third term is positive due to its quadratic nature and the fact that $m_i > 0$. By utilizing the equation (2.3) and the constraints b_v and b_a, we can express the derivative of V_{i1} as

$$\begin{aligned}
\dot{V}_{i1} =& \frac{\alpha_i}{\xi_i} z_i^T P w_i + m_i w_i^T \left(-\frac{\alpha_i}{\xi_i m_i} P z_i + \frac{\beta_i \xi_i}{m_i} h_i \right. \\
&\left. + \frac{1}{m_i} \frac{P z_i}{\xi_i (z_i^T P z_i - 1)} - \frac{\gamma}{m_i}(v_i - \hat{v}_T^i) + a_T^i - a_T \right) \\
&- \frac{z_i^T P w_i}{\xi_i (z_i^T P z_i - 1)} \\
=& \frac{\alpha_i}{\xi_i} z_i^T P w_i + \left(-\frac{\alpha_i}{\xi_i} P w_i^T z_i + \beta_i \xi_i w_i^T h_i \right. \\
&+ \frac{w_i^T P z_i}{\xi_i (z_i^T P z_i - 1)} - w_i^T \gamma (v_i - \hat{v}_T^i) \\
&\left. + m_i w_i^T (a_T^i - a_T)\right) - \frac{z_i^T P w_i}{\xi (z_i^T P z_i - 1)} \\
=& \beta_i \xi_i w_i^T h_i - w_i^T \gamma (v_i - \hat{v}_T^i) + m_i w_i^T (a_T^i - a_T) \\
\leq& \beta_i \xi_i n\sigma ||w_i|| - \gamma ||w_i||^2 + \gamma ||w_i|| b_v + m_i ||w_i|| b_a
\end{aligned}$$

It is evident that if the condition $||w_i|| > b_v + (\xi_i \beta_i n\sigma + m_i b_a)/\gamma$ is satisfied, then $\dot{V}_{i1} < 0$ holds, and the desired outcome is achieved. □

In the previous argument, we made use of the limits on the estimate errors and the fact that the norm of $h_i(t)$ is less than or equal to $n\sigma$, where σ is the limit on the repulsion as defined in equation (2.7), and n denotes the total quantity of agents.

Here, we provide demonstration that the i-th agent eventually enters the containment area and continues to stay within the ellipsoidal ring established by the containment and distancing regions using the control law introduced in (2.5).

Theorem 1. Take into account the group of agents defined by the mathematical representation in equation (2.3), with the governing rule specified in equation (2.5). Let's assume that at time t_0, the i-th agent begins outside the containment region represented by the ellipsoid $\mathcal{E}\left(P/c^2, x_T(t_0)\right)$, where:

$$c > \underline{c}(b_v, b_a) = \max_{i=1,2,\ldots,n} \left\{ 1, \frac{m_i \left\| \sqrt{P} \right\| (m_i b_a + \gamma b_v)}{\gamma^2} \right\}. \tag{2.10}$$

If the control parameters are chosen as

$$\alpha_i > \max\left\{\overline{\alpha}_i, W_0(1/e)\right\} \tag{2.11}$$

where

$$\overline{\alpha}_i = \frac{1}{c^2 - 1} + \frac{\left\| \sqrt{P}^{-1} \right\| \xi_i \left(b_v \gamma + b_a m_i + \beta_i n \sigma \xi_i\right)}{c} \tag{2.12}$$

then swarm member i will asymptotically enter the containment region, remain indefinitely in that area.

Proof. Consider the function $V_{i2} = \frac{1}{2}(m_i w_i + \gamma z_i)^T (m_i w_i + \gamma z_i)$. Its derivative along the trajectories of the model in (2.3) under the control law in (2.5) becomes

$$\begin{aligned}
\dot{V}_{i2} &= (m_i w_i + \gamma z_i)^T (m_i \dot{w}_i + \gamma \dot{z}_i) \\
&= (m_i w_i + \gamma z_i)^T \Big(u_i - m_i a_T + \gamma w_i \Big) \\
&= (m_i w_i + \gamma z_i)^T \Bigg(\frac{1}{\xi_i} \left(-\alpha_i P z_i + \frac{P z_i}{z_i^T P z_i - 1} \right) \\
&\quad - \gamma (v_i - \hat{v}_T^i) + m_i \hat{a}_T^i + \xi_i \beta_i h_i - m_i a_T + \gamma (v_i - v_T) \Bigg) \\
&= (m_i w_i + \gamma z_i)^T \Bigg(\frac{-\alpha_i}{\xi_i} P z_i + \frac{1}{\xi_i} \frac{P z_i}{z_i^T P z_i - 1} \\
&\quad - \gamma (v_T - \hat{v}_T^i) + m_i (\hat{a}_T^i - a_T) + \xi_i \beta_i h_i \Bigg) \\
&= \Bigg(\frac{-m_i \alpha_i}{\xi_i} w_i^T P z_i - \frac{\gamma \alpha_i}{\xi_i} z_i^T P z_i + \frac{m_i}{\xi_i} \frac{w_i^T P z_i}{z_i^T P z_i - 1} \\
&\quad + \frac{\gamma}{\xi_i} \frac{z_i^T P z_i}{z_i^T P z_i - 1} - (m_i \gamma w_i^T + \gamma^2 z_i^T)(v_T - \hat{v}_T^i) \\
&\quad + (m_i^2 w_i^T + \gamma m_i z_i^T)(\hat{a}_T^i - a_T) + (m_i w_i^T + \gamma z_i^T) \xi_i \beta_i h_i \Bigg)
\end{aligned}$$

Defining $Y_i = \sqrt{P} z_i$ and $Q_i = \sqrt{P} w_i$ we achieve

$$\begin{aligned}
\dot{V}_{i2} = &\frac{-m_i \alpha_i}{\xi_i} Q_i^T Y_i - \frac{\gamma \alpha_i}{\xi_i} Y_i^T Y_i + \frac{m_i}{\xi_i} \frac{Q_i^T Y_i}{Y_i^T Y_i - 1} \\
&+ \frac{\gamma}{\xi_i} \frac{Y_i^T Y_i}{Y_i^T Y_i - 1} - (m_i \gamma Q_i^T \sqrt{P}^{-1} + \gamma^2 Y_i^T \sqrt{P}^{-1})(v_T - \hat{v}_T^i) \\
&+ (m_i^2 Q_i^T \sqrt{P}^{-1} + \gamma m_i Y_i^T \sqrt{P}^{-1})(\hat{a}_T^i - a_T) \\
&+ (m_i Q_i^T \sqrt{P}^{-1} + \gamma Y_i^T \sqrt{P}^{-1}) \xi_i \beta_i h_i
\end{aligned}$$

We utilized the symmetry of P (and hence $\sqrt{P}$) in our reasoning. If we assume that α_i is greater than $W_0(1/e)$, and we apply the result from Lemma 2, we can conclude that $||Q_i||$ is less than or equal to $||\sqrt{P}||\ ||w_i||$, which is also less than or equal to $||\sqrt{P}||\ ||\overline{w}_i||$. It is

important to mention that, because the agent is located beyond the distancing region, the inequality $z_i^T P z_i > 1$ is true. Next, the derivative $\dot{V}_{i2}$ can be constrained from above.

$$\begin{aligned}\dot{V}_{i2} \leq & \frac{m_i\alpha_i}{\xi_i}\left\|\sqrt{P}\right\|\overline{w}_i\|Y_i\| - \frac{\gamma\alpha_i}{\xi_i}\|Y_i\|^2 + \frac{m_i}{\xi_i}\frac{\left\|\sqrt{P}\right\|\overline{w}_i\|Y_i\|}{\|Y_i\|^2-1} \\ & + \frac{\gamma}{\xi_i}\frac{\|Y_i\|^2}{\|Y_i\|^2-1} + (m_i\gamma\left\|\sqrt{P}\right\|\overline{w}_i\left\|\sqrt{P}^{-1}\right\| + \gamma^2\|Y_i\|\left\|\sqrt{P}^{-1}\right\|)b_v \\ & + (m_i^2\left\|\sqrt{P}\right\|\overline{w}_i\left\|\sqrt{P}^{-1}\right\| + \gamma m_i\|Y_i\|\left\|\sqrt{P}^{-1}\right\|)b_a + m_i\beta_i\xi_i\left\|\sqrt{P}\right\|\overline{w}_i\left\|\sqrt{P}^{-1}\right\|n\sigma \\ & + \gamma\beta_i\xi_i\|Y_i\|\left\|\sqrt{P}^{-1}\right\|n\sigma\end{aligned}$$

It should be noted that if the swarm member i is not located inside the ellipsoidal zone described by $P/c^2, c > 1$,

$$z_i^T P z_i - 1 \geq c^2 - 1 \Rightarrow \frac{1}{z_i^T P z_i - 1} \leq \frac{1}{c^2-1}$$

is satisfied. By utilizing this feature, we obtain

$$\dot{V}_{i2} \leq k_1||Y_i||^2 + k_2||Y_i|| + k_3 \tag{2.13}$$

where

$$\begin{aligned}k_1 &= -\frac{\gamma}{\xi_i}\left(\alpha_i - \frac{1}{c^2-1}\right) \\ k_2 &= \frac{m_i\alpha_i}{\xi_i}\overline{w}_i\left\|\sqrt{P}\right\| + \frac{m_i\left\|\sqrt{P}\right\|\overline{w}_i}{\xi_i(c^2-1)} + \gamma^2\left\|\sqrt{P}^{-1}\right\|b_v + \gamma m_i\left\|\sqrt{P}^{-1}\right\|b_a + \gamma\beta_i\xi_i n\sigma\left\|\sqrt{P}^{-1}\right\| \\ k_3 &= m_i\gamma\left\|\sqrt{P}\right\|\overline{w}_i\left\|\sqrt{P}^{-1}\right\|b_v + m_i^2\left\|\sqrt{P}\right\|\overline{w}_i\left\|\sqrt{P}^{-1}\right\|b_a + m_i\beta_i\xi_i\left\|\sqrt{P}\right\|\overline{w}_i\left\|\sqrt{P}^{-1}\right\|n\sigma \\ &= m_i\overline{w}_i\left\|\sqrt{P}\right\|\left\|\sqrt{P}^{-1}\right\|\left(\gamma b_v + m_i b_a + \xi_i\beta_i n\sigma\right)\end{aligned}$$

The expression on the right side of equation (2.13) represents a parabola with respect to the magnitude of Y_i. Put simply, $\dot{V}_{i2}$ is limited by a parabolic curve in relation to the variable $||Y_i||$, which is determined by the coefficients k_1, k_2, k_3. Given that c is greater than 1 and assuming that α_i is greater than $\frac{1}{(c^2-1)}$, it follows that k_1 is less than 0 and k_2 and k_3 are greater than 0. On the RHS, the sign of the two roots are different. As the function

depends on the magnitude of $||Y_i||$, only the positive root r_1 is an acceptable solution. By solving the equation, the value of r_1 can be determined.

$$r_1 = \frac{(c^2-1)\left\|\sqrt{P}^{-1}\right\|\xi_i\Big(b_v\gamma + b_a m_i + \beta_i n\sigma\xi_i\Big)}{\alpha_i(c^2-1)-1}.$$

Then, by imposing $c > r_1$, it follows that $\dot{V}_{i2} < 0$ if

$$\alpha_i > \frac{1}{c^2-1} + \frac{\left\|\sqrt{P}^{-1}\right\|\xi_i\Big(b_v\gamma + b_a m_i + \beta_i n\sigma\xi_i\Big)}{c}.$$

Since this holds as long as $z_i^T P z_i > c^2$, we conclude that the agents will enter the ellipsoid $\mathcal{E}(P/c^2, x_T(t))$. □

The repulsive impact arising from the distance region, given by the term $\frac{Pz_i(t)}{\xi_i\left(z_i^T(t)Pz_i(t)-1\right)}$, increases indefinitely as the agents approach the distancing region. As the agents go closer to the boundary of this region, this particular term in the control law becomes more important than other terms. This prevents the agents from trespassing the distancing region. If the value α_i is chosen to be bigger than the given lower limit $\overline{\alpha}_i$, the agents will definitely enter and stay within the containment regions.

In the section below, we elaborate the implementation of the algorithm on a group of quadcopters.

2.2 Quadcopter Model

2.2.1 quadcopter Model and Control

Our approach for a swarm of quadcopters incorporates the paradigm outlined in Mellinger et al. [2012], Toksöz et al. [2019], Merzi et al. [2022].

$$\begin{aligned} m\ddot{p} &= F_g + R^W F_q \\ I\dot{\Omega} &= -\Omega \times I\Omega + \tau \end{aligned} \tag{2.14}$$

In this scenario, $p = [x, y, z]^\top \in \mathbb{R}^3$ denotes the quadcopter's location in the global Cartesian frame, whereas $\Omega = [\bar{p}, \bar{q}, \bar{r}]^\top \in \mathbb{R}^3$ indicates its angular velocity. The variable m represents the mass of the quadcopter, and $I \in \mathbb{R}^{3\times3}$ signifies its inertia tensor. The gravitational force vector, denoted as F_g, can be expressed as $F_g = [0, 0, -mg]^\top \in \mathbb{R}^3$, where g represents the gravitational acceleration constant. This force always acts in the direction opposite to the positive z-axis of the global inertial frame. The quadcopter's thrust vector, denoted as $F_q = [0, 0, F_{tot}]^\top \in \mathbb{R}^3$, represents the overall thrust created by the rotors. The thrust is always aligned with the z-axis of the quadcopter body frame. The symbol τ represents the torque generated by the rotors, and it belongs to the set of real numbers $\mathbb{R}^3$. The control inputs to the quadcopter dynamics are F_q and τ, which are influenced by the rotor speeds. Since the forces operating on the quadcopter are specified in the body frame, while the motion is given in the global frame, it is essential to convert the body forces into the global (world) frame. The transformation is accomplished by utilizing the rotation matrix $R^W \in \mathbb{R}^{3\times3}$, which converts the body frame to the global (inertial, world) frame.

Figure 2.3 depicts a possible arrangement of a quadcopter, showcasing the body forces generated by its rotors.

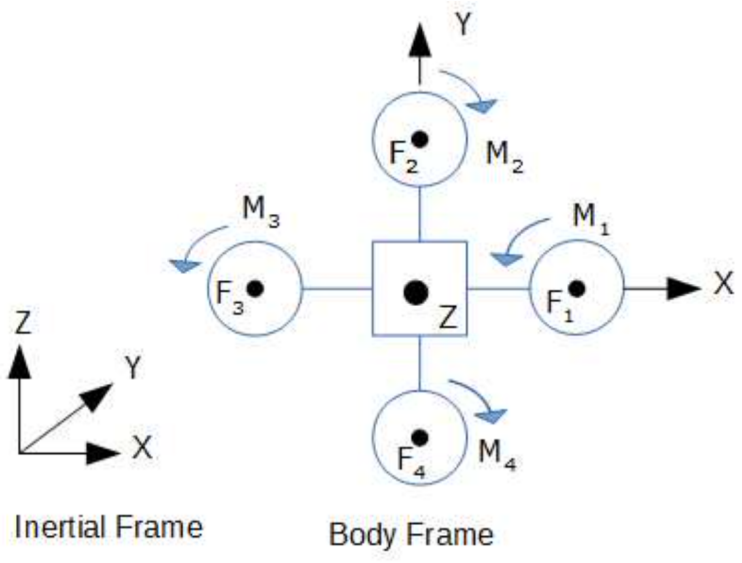

Figure 2.3: quadcopter configuration and body forces. (Figure taken from Toksöz et al. [2019].)

The separate rotors provide forces of thrust in the z-axis of the quadcopter body frame, shown as $F_i, i = 1, \ldots, 4$ in Figure 2.3. Furthermore, they generate rotational moments according to their spin direction, denoted as $M_i, i = 1, \ldots, 4$ in Figure 2.3. Normally, a quadcopter has two rotors that rotate in a clockwise direction and two rotors that rotate in a counterclockwise direction. This configuration helps to maintain balance and avoids the quadcopter from constantly rotating around its z-axis. The force and moment produced by each rotor, denoted by $i = 1, \ldots, 4$, can be computed using the following equations:

$$\begin{aligned} F_i &= k_F \omega_i^2, \\ M_i &= k_M \omega_i^2, \end{aligned} \tag{2.15}$$

The variables k_F and k_M reflect the force and moment characteristics of the motors, respectively. These characteristics are determined by the features of the motor and propeller. The variable ω_i represents the angular velocities of the rotors, measured in radians per second (rad/s). The aggregate thrust produced by the rotors can be determined by adding together the individual thrusts generated by each rotor.

$$F_{tot} = F_1 + F_2 + F_3 + F_4 = k_F \sum_{i=1}^{4} \omega_i^2, \tag{2.16}$$

The noted previously, the force operates along the z-axis of the quadcopter's body frame. If the forces F_i and moments M_i for all rotors $i = 1, \ldots, 4$ are equivalent, then the quadcopter experiences no rotating forces. Nevertheless, any disparities between these forces or moments lead to rotational moments around the axes of the quadcopter body frame, which can be calculated in the following manner:

$$\begin{aligned} \tau_\phi &= l\left(-F_4 + F_2\right) = l k_F \left(\omega_2^2 - \omega_4^2\right), \\ \tau_\theta &= l\left(-F_1 + F_3\right) = l k_F \left(-\omega_1^2 + \omega_3^2\right), \\ \tau_\psi &= -M_2 + M_1 - M_4 + M_3 = k_M(\omega_1^2 - \omega_2^2 + \omega_3^2 - \omega_4^2). \end{aligned} \tag{2.17}$$

where l represents the distance between the rotors that are placed directly opposite each other, specifically rotors 1 and 3, as well as rotors 2 and 4. As seen in Figure 2.3, τ_ϕ, τ_θ, and τ_ψ denote the moments around the x, y, and z axes of the body frame, respectively. These moments cause the body to undergo roll, pitch, and yaw movements. The roll, pitch, and yaw angles are denoted as ϕ, θ, and ψ, respectively.

Additionally, we incorporate the dynamics of the DC motors by representing them as basic first-order systems, expressed in the following format:

$$\dot{\omega}_i = -\tau_i \left(\omega_i - \omega_i^{des}\right), \quad i = 1, \ldots, 4, \tag{2.18}$$

The symbol τ_i represents the motor gains, where $1/\tau_i$ represents the time constants for the motors. To simplify matters, we use the assumption in this work that all motors are the same, so $\tau_i = \tau_m$ for a certain value of τ_m and for all $i = 1, \ldots, 4$. In equation (2.18), ω_i^{des} denotes the angular speeds that the quadcopter controllers select as the desired values for the rotors.

Different techniques can be employed to illustrate the alignment of the body frame with respect to the world frame. The Z-X-Y and Z-Y-X Euler angle representations are frequently encountered in academic literature. Each depiction results in distinct formulations of the rotation matrix R^W. As a result, there are several equations for the relationship between the angular velocity $\Omega = [\bar{p}, \bar{q}, \bar{r}]^\top$ and the Euler angle rates $[\dot{\phi}, \dot{\theta}, \dot{\psi}]$. Moreover, this leads to subtle variations in the manifestations of the control words.

This study employs the Z-Y-X Euler angles representation. The rotation matrix R^W for this representation is defined in terms of the Euler angles (roll ϕ, pitch θ, and yaw ψ).

$$R^W = \begin{bmatrix} c_\theta c_\psi & s_\phi s_\theta c_\psi - c_\phi s_\psi & c_\phi s_\theta c_\psi + s_\phi s_\psi \\ c_\theta s_\psi & s_\phi s_\theta s_\psi + c_\phi c_\psi & c_\phi s_\theta s_\psi - s_\phi c_\psi \\ -s_\theta & s_\phi c_\theta & c_\phi c_\theta \end{bmatrix} \tag{2.19}$$

where s_ℓ and c_ℓ stand for $\sin(\ell)$ and $\cos(\ell)$, respectively, with ℓ representing the Euler angles ϕ, θ, and ψ.

This paper utilizes a feedback linearization-based controller to regulate the attitude, altitude, and position of the quadcopters. The approach is similar to the one described in Toksöz et al. [2019]. The attitude controller functions within the inner loop, while the altitude and position controllers operate within the outer loop of the overall cascade controller structure. quadcopter control commonly employs cascade control structures, which rely on singular perturbation theory as described in Roussel [2019]. Their assumption is based on the fact that the inner loop operates at a significantly higher speed (with a wider loop bandwidth) than the outer loop and is exponentially stable Baca et al. [2021]. This assumption enables the development of the outer loop controller without the requirement to

consider the dynamics of the inner loop. The subsequent sections provide a comprehensive explanation of the altitude, attitude, and position controls.

Altitude Control: Based on the dynamics along the z-axis described in (2.14), the altitude controller is constructed using a feedback linearizing technique.

$$F_{tot} = (g + u_z) \frac{m}{\cos(\theta)\cos(\phi)} \tag{2.20}$$

here g accounts for effects of gravity. The variable u_z specifically tailored to attain and sustain a predetermined height for the members. The controller mentioned above takes us to below:

$$u_z = -k_{p,z}(z - z_d) - k_{d,z}(\dot{z} - \dot{z}_d) + \ddot{z}_d \tag{2.21}$$

By carefully choosing the controller gains $k_{p,z}$ and $k_{d,z}$ and given that the angles ϕ and θ are insignificant, it can be ensured that the quadcopter will climb to the required height. The stated altitude trajectory is determined by the values of z_d, $\dot{z}_d$, and $\ddot{z}_d$. When the intended altitude remains constant, both the rate of change of altitude ($\dot{z}_d$) and the acceleration of altitude ($\ddot{z}_d$) are zero. In this case, the controller can be seen as a proportional controller with velocity damping. The calculated F_{tot} in (2.20) essentially indicates a target thrust that needs to be attained by modifying the rotor speeds.

Attitude Control: The use of a feedback linearization-based technique is also viable for the attitude control of a quadcopter. To achieve this objective, we use the approach outlined in the publication of Toksoz et al. Toksöz et al. [2019]. The quadcopter's symmetric construction results in its inertia tensor having a diagonal shape in relation to its body frame, represented as $I = \text{diag}\{I_{xx}, I_{yy}, I_{zz}\}$. In addition, given the selected Z-Y-X Euler angles representation, the angular velocity vector $\Omega = [\bar{p}, \bar{q}, \bar{r}]$.The transpose of Ω may be represented using the Euler angle rates $[\dot{\phi}, \dot{\theta}, \dot{\psi}]^T$ in the following manner:

$$\Omega = \begin{bmatrix} \bar{p} \\ \bar{q} \\ \bar{r} \end{bmatrix} = \begin{bmatrix} 1 & 0 & -s_\theta \\ 0 & c_\phi & c_\theta s_\phi \\ 0 & -s_\phi & c_\theta c_\phi \end{bmatrix} \begin{bmatrix} \dot{\phi} \\ \dot{\theta} \\ \dot{\psi} \end{bmatrix} \tag{2.22}$$

By inserting these expressions into the angular dynamics equation in (2.14) and modifying them (assuming modest angles), one may derive the feedback linearized controllers in the

following manner:

$$\begin{aligned}\tau_\phi &= \left(u_\phi + u_\phi^{pd}\right)\frac{I_{xx}}{l}\\ \tau_\theta &= \left(u_\theta + u_\theta^{pd}\right)\frac{I_{yy}}{l}\\ \tau_\psi &= \left(u_\psi + u_\psi^{pd}\right)I_{zz}\end{aligned} \tag{2.23}$$

where u_ϕ, u_θ, u_ψ are given by

$$\begin{aligned}u_\phi &:= \dot{\theta}\dot{\psi}\frac{I_{yy} - I_{zz}}{I_{xx}} - \dot{\theta}\omega_r\frac{J_r}{I_{xx}}\\ u_\theta &:= \dot{\phi}\dot{\psi}\frac{I_{zz} - I_{xx}}{I_{yy}} + \dot{\phi}\omega_r\frac{J_r}{I_{yy}}\\ u_\psi &:= \dot{\phi}\dot{\theta}\frac{I_{xx} - I_{yy}}{I_{zz}}\end{aligned} \tag{2.24}$$

The rotor's inertia is represented by the symbol J_r, while $w_r = -w_1 + w_2 - w_3 + w_4$. It is crucial to acknowledge that the sign of each w_i is contingent upon the rotational direction of the associated rotor.

The controllers that correspond to the rotational dynamics may be specified in the following manner:

$$\begin{aligned}u_\phi^{pd} &= -k_{p,\phi}\left(\phi - \phi_d\right) - k_{d,\phi}\left(\dot{\phi} - \dot{\phi}_d\right) + \ddot{\phi}_d\\ u_\theta^{pd} &= -k_{p,\theta}\left(\theta - \theta_d\right) - k_{d,\theta}\left(\dot{\theta} - \dot{\theta}_d\right) + \ddot{\theta}_d\\ u_\psi^{pd} &= -k_{p,\psi}\left(\psi - \psi_d\right) - k_{d,\psi}\left(\dot{\psi} - \dot{\psi}_d\right) + \ddot{\psi}_d\end{aligned} \tag{2.25}$$

The symbols ϕ, θ, and ψ denote the Euler angles, whereas $\dot{\phi}$, $\dot{\theta}$, and $\dot{\psi}$ indicate their corresponding rates. The symbols ϕ_d, θ_d, and ψ_d represent the desired Euler angles. The symbols $\dot{\phi}_d$, $\dot{\theta}_d$, and $\dot{\psi}_d$ represent the desired rates, and $\ddot{\phi}_d$, $\ddot{\theta}_d$, and $\ddot{\psi}_d$ represent the corresponding desired accelerations.

Citing Mallinger Mellinger et al. [2012] and assuming that the quadcopter is in a stationary position (with roll and pitch angles, ϕ and θ, equal to zero), the position controllers' outputs may be transformed into the required angles as follows:

$$\begin{aligned} \phi_d &= \frac{1}{g}\left(u_x \sin(\psi) - u_y \cos(\psi)\right) \\ \theta_d &= \frac{1}{g}\left(u_x \cos(\psi) + u_y \sin(\psi)\right) \end{aligned} \tag{2.26}$$

The position controllers for the Cartesian coordinates (x, y) are denoted as u_x and u_y, and will be further explained in the next discussion. In this study, we designate the required yaw angle as $\psi_d = 0$. In addition, we maintain fixed roll and pitch angles and assume that the rates of change and accelerations of these angles are all zero.

Position Control in the Cartesian Space: The outer loops in quadcopter control systems are considered to be the position controllers for the (x, y) coordinates in the Cartesian space. In this case, we use traditional proportional-derivative controllers with additional feedforward components, as explained in equation (2.27). The control terms u_x and u_y are produced in the following manner:

$$\begin{aligned} u_x &= -k_{p,x}\left(x - x_d\right) - k_{d,x}\left(\dot{x} - \dot{x}_d\right) + \ddot{x}_d \\ u_y &= -k_{p,y}\left(y - y_d\right) - k_{d,y}\left(\dot{y} - \dot{y}_d\right) + \ddot{y}_d \end{aligned} \tag{2.27}$$

The controller parameters are denoted as k_p and k_d. The PD controller's outputs, u_x and u_y, are used in equation (2.26) to calculate the desired angles. The sets $\{x_d, \dot{x}_d, \ddot{x}_d\}$ and $\{y_d, \dot{y}_d, \ddot{y}_d\}$ denote the intended paths in the (x, y) plane. In the context of quadcopter tasks, these paths may be created by using suitable route planning or path generating algorithms.

Rotor Speed Control: After calculating all the control terms, the final stage involves solving (2.16) and (2.17) simultaneously to obtain the squared desired rotor speeds as follows:

$$\begin{bmatrix} \left(\omega_1^{\text{des}}\right)^2 \\ \left(\omega_2^{\text{des}}\right)^2 \\ \left(\omega_3^{\text{des}}\right)^2 \\ \left(\omega_4^{\text{des}}\right)^2 \end{bmatrix} = \frac{1}{k_F} \begin{bmatrix} 1 & 1 & 1 & 1 \\ 0 & l & 0 & -l \\ -l & 0 & l & 0 \\ \kappa & -\kappa & \kappa & -\kappa \end{bmatrix}^{-1} \begin{bmatrix} F_{tot} \\ \tau_\phi \\ \tau_\theta \\ \tau_\psi \end{bmatrix} \tag{2.28}$$

where $\kappa = k_M / k_F$. As described in Toksöz et al. [2019], the desired rotor speeds can be saturated between previously set min. and max. values, which are typically set to be positive or zero constants. The rotor turning speed that we want to achieve ω_i^{des}, then

calculated by taking the root of the computed values. These desired speeds are applied as inputs to the motor dynamics in (2.18).

Overall Procedure: In summary, the whole process may be outlined as follows.

(i) By using the double integrator agent model described in equation (2.1) and utilizing the control law specified in equation (2.5), determine the intended path $\{x_d, \dot{x}_d, \ddot{x}_d\}$ and $\{y_d, \dot{y}_d, \ddot{y}_d\}$ in the (x, y) plane. Use this path in equation (2.27) to calculate u_x and u_y.

(ii) To determine the altitude controller u_z, we need to input either a constant desired altitude z_d or a desired altitude trajectory $\{z_d, \dot{z}_d, \ddot{z}_d\}$ into equation (2.21).

(iii) Calculate the desired angular rates using the values of u_x and u_y obtained from equation (2.27), according to equation (2.26). Compute the control inputs u_ϕ^{pd}, u_θ^{pd}, and u_ψ^{pd} using the rates provided in equation (2.25).

(iv) Determine the values of u_ϕ, u_θ, and u_ψ by using equation (2.24).

(iv) Compute the values of u_ϕ, u_θ, and u_ψ using (2.24).

(v) Calculate the desired torques using (2.23).

(vi) Determine the desired thrust using (2.20).

(vii) To acquire the desired motor speeds, calculate equations (2.16) and (2.17) concurrently, using the desired thrust and desired torques.

(viii) Utilize the computed target motor speeds as input for the motor controllers. In our instance, this is accomplished by implementing them to the motor dynamics in (2.18), guaranteeing that the rotors rotate at these velocities and the intended performance is attained.

It is important to reiterate that the double integrator dynamics model functions as a path planner for the quadcopter platform. Subsequently, appropriate low-level controllers are employed to guarantee that the quadcopters accurately follow the paths that have been established. Consequently, the theoretical findings obtained for the double integrator agent model may be applied to the group of quadcopters. Within this particular framework, the dynamics of the double integrator agent serves as a model that demonstrates the feasibility of the swarm of quadcopter (or agents that have different dynamics).

2.3 Simulation Results

This part presents a comprehensive analysis of numerical simulations, corroborating the behavioral patterns discussed previously. Our primary objective is to demonstrate the significant influence of SVO parameters on agent actions. All simulations were conducted using MATLAB. However, it's noteworthy that other dynamic simulation tools, such as ROS/Gazebo as demonstrated in Merzi et al. [2022], could yield comparable qualitative results. The agents in our simulations are represented by Crazyflie 2.0 quadcopters, and the specific characteristics of these agents, as well as the parameters of the controllers used, are provided in Table 2.1.

Parameter	Value
m	$0.033\ kg$
l	$39.73e^{-3}\ m$
I_{xx}	$1.395e^{-5}\ kgm^2$
I_{yy}	$1.436e^{-5}\ kgm^2$
I_{zz}	$2.173e^{-5}\ kgm^2$
J_r	$0\ kgm^2$
ω_{min}	$0\ rad/s$
ω_{max}	$3000\ rad/s$
k_F	$2.8799e^{-8}$
k_M	$7.2385e^{-10}$
τ_m	$20\ s^{-1}$
$k_{p,x},\ k_{p,y}$	2
$k_{d,x},\ k_{d,y}$	10
$k_{p,\phi},\ k_{p,\theta},\ k_{p,\psi}$	40
$k_{p,z}$	6
$k_{d,\phi},\ k_{d,\theta},\ k_{d,\psi}$	6
$k_{d,z}$	6

Table 2.1: Quadcopter and Controller Parameters

Within our simulations, we examine two separate possibilities. In the first case, the target remains still, but in the subsequent situation, the target travels in a circular path. Both situations involve the movements of agents with different degrees of sociality. Our simulations demonstrate that the agents effectively converge inside the containment region, and perfectly stay outside the distancing region. They consistently stay within the ellipsoidal ring, regardless of their social preferences. Those simulation results backs up the

analytical findings. Furthermore, the simulations show that altering the SVO parameter, which represents distinct social preferences, leads to a range of reactions from the agents. These responses are consistent with the analytical findings.

2.3.1 Example 1: Stationary Target

In this example, we examine a situation where the target is not moving, indicated by the fact that both the target's velocity (v_T) and acceleration (a_T) are equal to zero. Let us consider a swarm consisting of $n = 10$ agents, moving inside a three-dimensional space. The shaping matrix for the ellipsoidal areas (distancing and containment regions) was constructed using the diagonal matrix $P = \text{diag}(1/9, 1/4)$. The control rule specified in equation (2.5) is implemented using a velocity damping coefficient of $\gamma = 60$. When the target's velocity is zero, $\gamma = 60$ serves as the damping coefficient. Otherwise, it would serve as the velocity matching coefficient. The remaining control parameters are assigned the values $\beta = 2$, $\alpha = 9$, and $c = 1.05$. The anticipated detection radius for repulsion between agents is $\sigma = 10$ meters. The target is located at an elevation of $z_d = 10$ meters. The quadcopter swarm has to rise to this elevation and capture/enclose the target in the (x, y) plane at this fixed elevation. In essence, the advanced controller functions in a two-dimensional manner, apart from the altitude controller. To simplify the situation, we use the assumption that the target does not move and is located at coordinates $(x, y) = (0, 0)$, with a distance of 10 meters from the observer in the vertical direction ($z_d = 10$ meters). At first, the agents are located outside the containment zone, and their initial (x, y) coordinates are given in Table 2.2. The agents are initially stationary on the ground, with a vertical position of $z_i = 0$ for $i = 1, \ldots, n$. Simulations were performed using different initial conditions. In this instance, the limits b_v and b_a are set to zero. The simulations were conducted until $t = 150$ seconds.

i	1	2	3	4	5
x	10	8.66	6.24	0	-6.24
y	0	6.24	8.66	10	8.66
i	6	7	8	9	10
x	-8.66	-10	-8.66	-6.24	0
y	6.24	0	-6.24	-8.66	-10

Table 2.2: Initial Positions of Agents

Within our simulation, we allocated distinct SVO parameters to each agent, spanning from 0.1 to 1.0. Figure 2.4 depicts the "elliptic distances" $z^T Pz$ of the agents in relation to the target. The plot shows that the SVO parameter has a substantial impact on the rate at which convergence occurs towards the containment zone. Agents with lower ξ values exhibit faster convergence. As an example, agent 1 with a value of $\xi_1 = 0.1$ reached the border of the distancing zone at roughly $t = 20$ seconds, whereas agent 10 with a value of $\xi_{10} = 1.0$ reached the boundary at around $t = 80$ seconds. The change in the speed at which convergence occurs is caused by the inverse impact of ξ on the attraction term towards the goal. However note that, SVO is not the only parameter that effects the convergence speed, since agents also interact among each other.

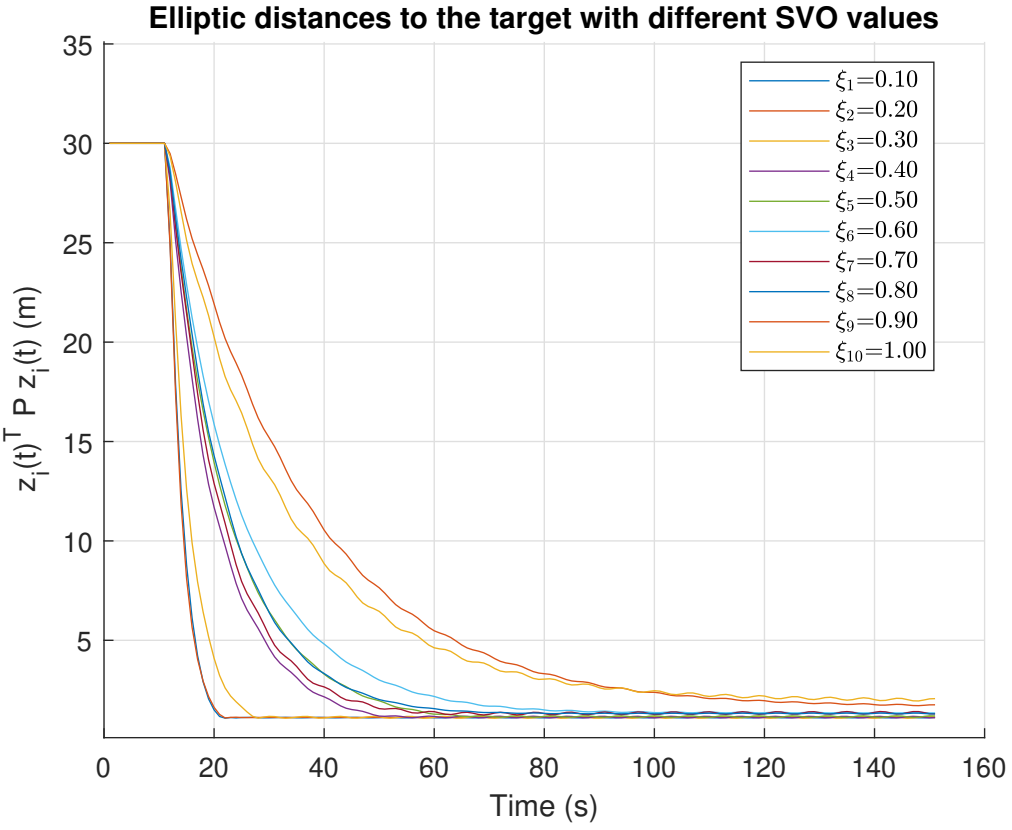

Figure 2.4: Elliptic distances $z^T Pz$ of the agents to the target.

The trajectories of the agents, beginning from their initial positions as specified in Table 2.2, are displayed in Figure 2.5 within the 3D space. Meanwhile, their trajectories in the (x, y) plane are illustrated in Figure 2.6.

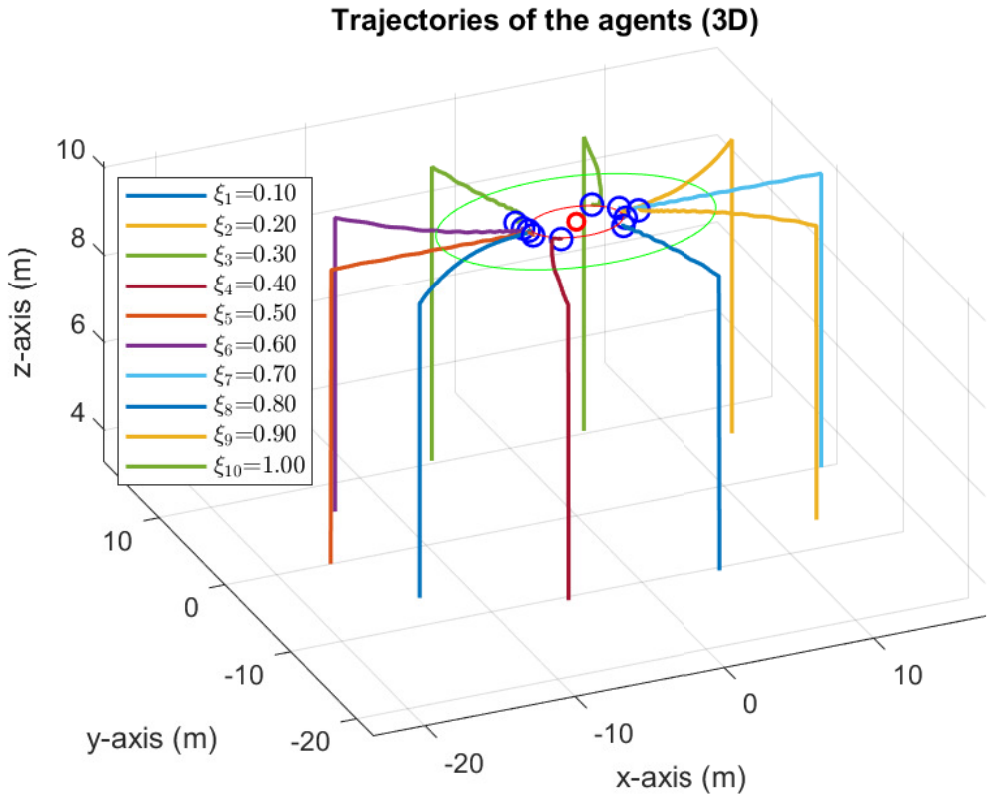

Figure 2.5: Trajectories in (x, y, z) of agents with different ξ values.

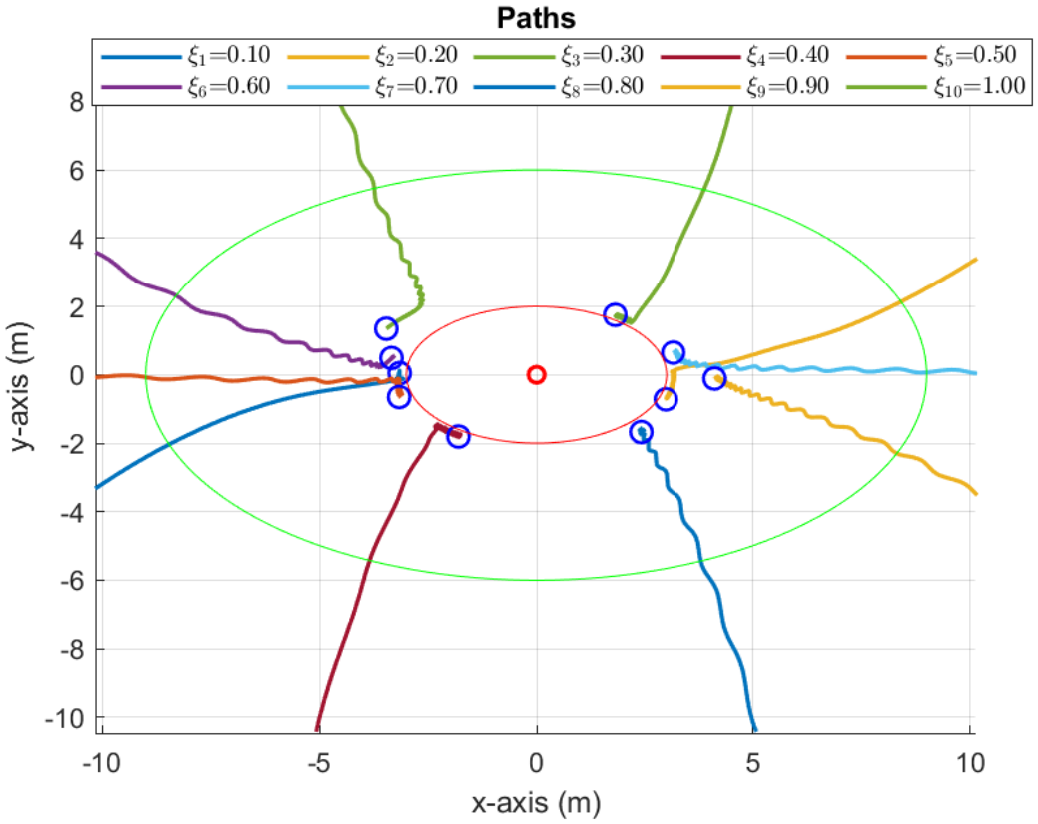

Figure 2.6: Trajectories in (x, y) of agents with different ξ values.

As seen in Figure 2.5, the agents effectively achieve the appropriate height and then proceed to orbit around the target. They enter the containment area and keep a safe distance from the designated distancing area, as expected. Furthermore, it is apparent that agents with smaller ξ_i values (showing a lower level of social orientation), which converge more rapidly as shown in Figure 2.4, have a tendency to navigate around the perimeter of the distancing zone. This behavior is caused by the influence exerted by the agents that arrived later and had higher ξ_i values, suggesting a stronger social orientation. The agents' delayed arrival is evident in Figure 2.4, since they are positioned further from the target according to the elliptical distance $z^T P z$.

The Figure 2.7 shows the magnitudes of the velocities of the agents relative to the target. From the image, it can be seen that the agents successfully reach a state of velocity consensus, where all relative velocities finally converge to zero. This suggests that the swarm

achieves a stable arrangement around the objective, regardless of the individuals' social preferences.

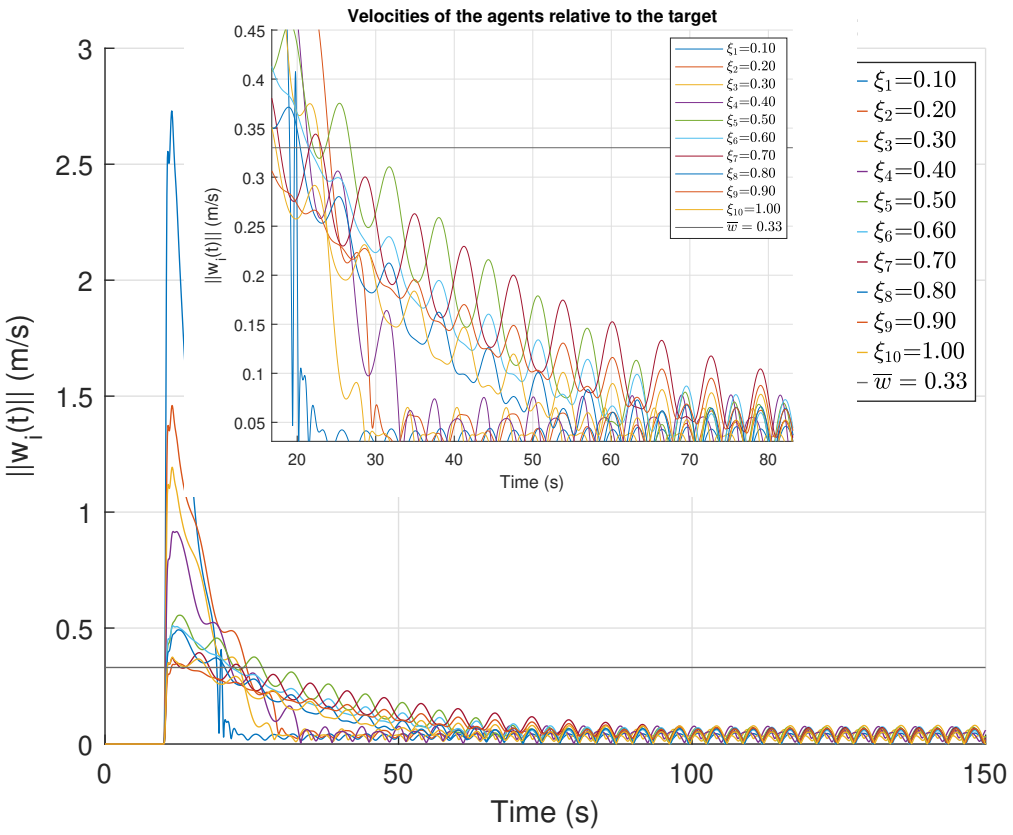

Figure 2.7: The rate at which velocities change in relation to the goal, denoted as $\|w_i(t)\|$. Ultimately, all of them converge to zero, resulting in a static configuration near the objective. There are 10 agents, each with distinct social preferences. The interval $t \in [20, 70]$ is magnified to enhance clarity.

2.3.2 Example 2: Mobile Target

In second example, we examine a moving object that follows a circular path. The physical characteristics of the quadcopters and the control settings remain same from Example 1. The path of the target is determined by a circular trajectory.

$$X_T = \begin{bmatrix} 0 \\ 0 \\ 10 \end{bmatrix} + 8 \begin{bmatrix} \cos 0.05t \\ \sin 0.05t \\ 0 \end{bmatrix}.$$

It is important to remember that in our technique, we make use of approximations for the velocity and acceleration of the target, since we presume that these values are not known. In this particular instance, we used

$$\hat{v}_T^i(t) = v_T(t) + b_v^i \cos(it) \tag{2.29}$$

$$\hat{a}_T^i(t) = a_T(t) + b_a^i \sin(it) \tag{2.30}$$

Given the values $v_T(t) = \dot{x}_T(t)$, $a_T(t) = \ddot{x}_T(t)$, $b_v = 0.05$, and $b_a = 0.1$, these are the estimates. The area of distance is determined by the same matrix $P = \text{diag}(1/9, 1/4)$ as in Example 1. The red ellipse symbolizes the zone of distance, while the green ellipse represents the region of containment. We once again use the initial agent locations specified in Table 2.2, and the simulations are carried out during the time span $t \in [0, 150]$ seconds.

Figure 2.8 illustrates the paths followed by the agents, together with the relevant ellipsoids. On the other hand, Figure 2.9 demonstrates the ellipsoidal distances $z^T P z$ to the target as time progresses. As expected, the agents gather in the containment area and stay there, while also avoiding the distancing area. Put simply, the swarm effectively catches and encloses the target inside the designated ellipsoidal ring.

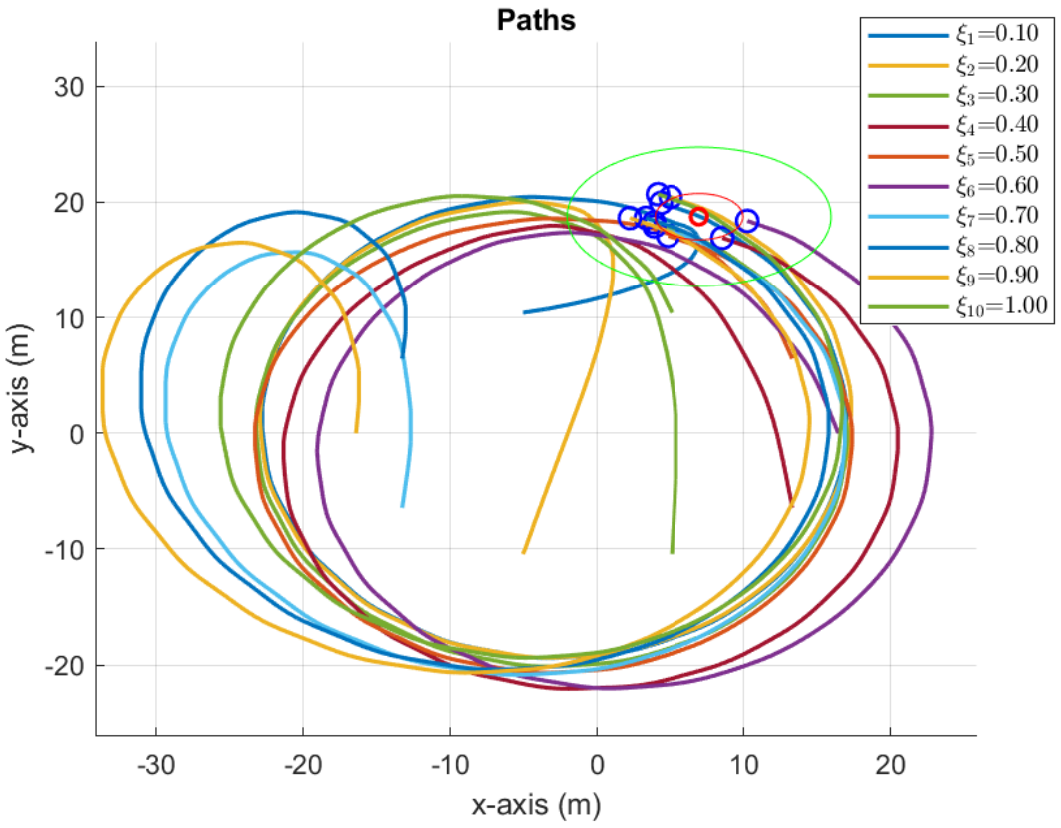

Figure 2.8: The paths of the agents as they track a target moving in a circular pattern.

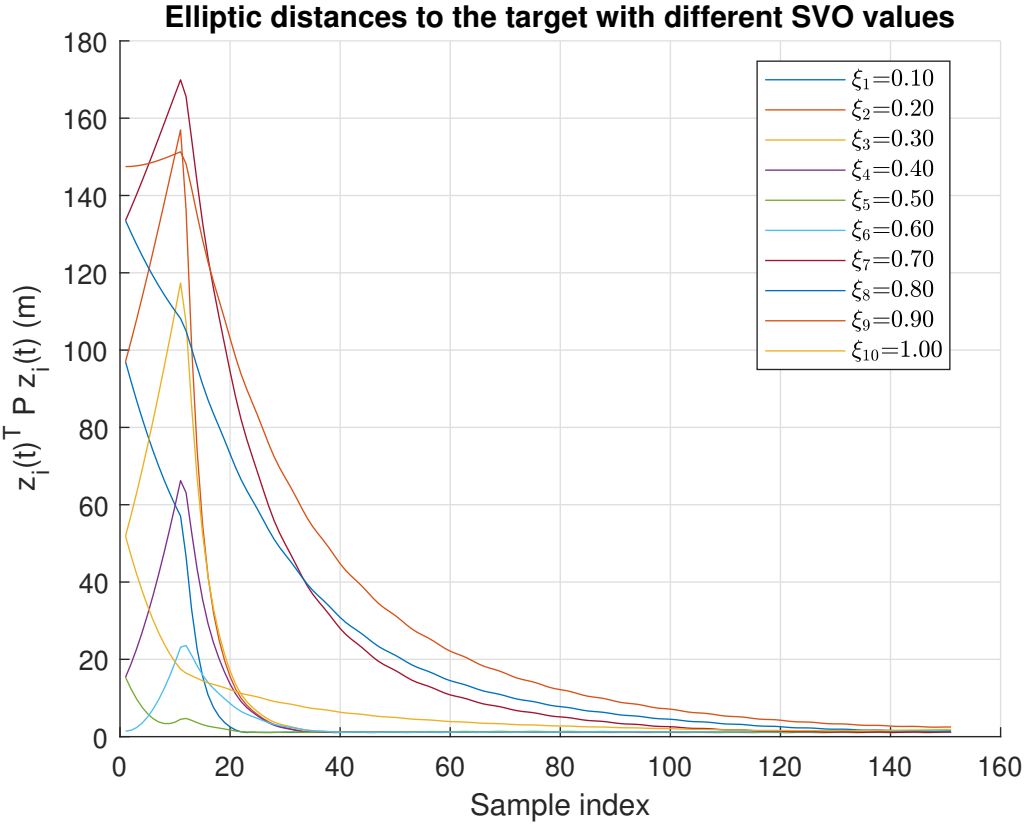

Figure 2.9: Calculate the elliptic distances to the objective for all agents. The agent with a social factor of $\xi_1 = 0.1$ reached the border of the distance zone significantly quicker, at around $t = 20$, compared to the agent with a social factor of $\xi_{10} = 1.0$, who reached the boundary much slower, at approximately $t = 120$.

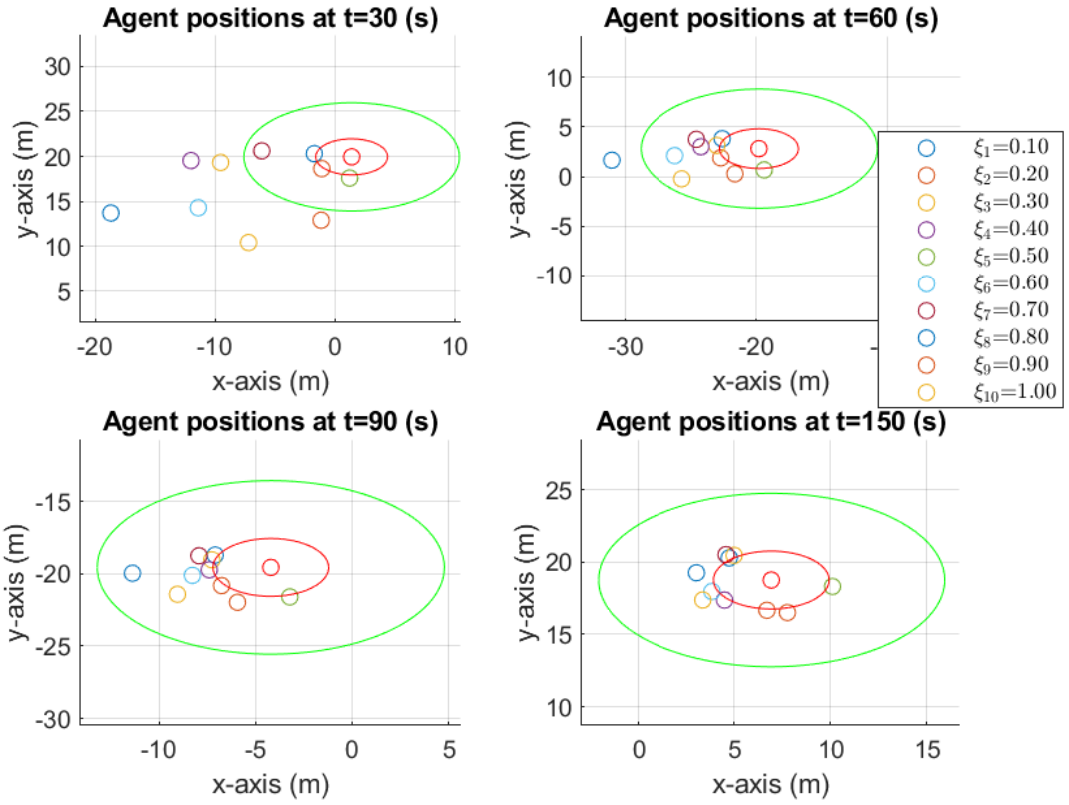

Figure 2.10: Visual representations of the agents' positions relative to the goal on a two-dimensional (x, y) plane.

Similar to the case when the target is not moving, it can be noticed that less social agents travel at a faster pace towards the target compared to the more sociable individuals. As seen in Figure 2.9, the less social agent, characterized by $\xi_9 = 0.1$, reached the border of the distancing area at around $t = 20$ seconds. On the other hand, the agent that exhibits social behavior, with $\xi_{10} = 1.0$, reached the boundary at roughly $t = 120$ seconds. Figure 2.10 displays snapshots of the agents' locations relative to the goal in the (x, y) plane at different time points throughout the experiment. The first agents that have arrived possess ξ values of 0.1, 0.2, 0.3, 0.4, and 0.5, as anticipated.

The Figure 2.11 illustrates the magnitudes of the relative velocities $\|w_i\|$ of the agents in relation to the target.

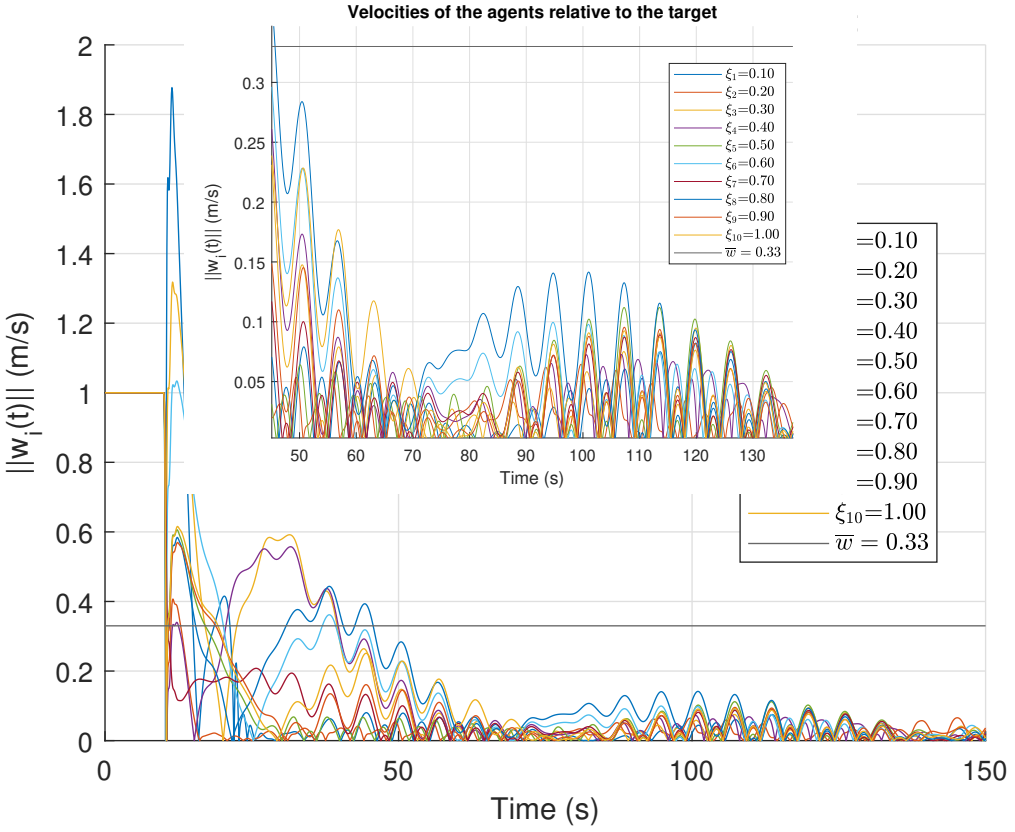

Figure 2.11: The magnitude of the relative velocities of the agents in relation to the target is denoted as $\|w_i\|$.

In summary, we conducted simulations for two distinct scenarios to validate our analytical findings. Our results confirm that incorporating SVO as a parameter into the control law slightly influences the agents' behavior. Despite the minor differences among agents caused by SVO, it is both theoretically guaranteed and verified through simulations that the agents converge within the containment region and do not breach the distancing region.

3. SVO WITH COORDINATE COUPLING MATRICES FOR SWARM FORMATION

This chapter incorporates SVO with coordinate coupling matrices. We have based our approach on the work by Fedele et al. [2022], which uses coordinate coupling matrices to guarantee the cohesiveness of a swarm within a polytopic region and ensures steady-state motion of agents in a rotational frame around the swarm centroid. The authors have introduced two coordinate coupling matrices that weight both the attractive and the repulsive interactions among agents.

In this chapter, we extend this framework by introducing the SVO parameter into the coordinate coupling matrices to observe its impact on agent behavior. Specifically, we hypothesized that assigning different SVO values to each team would result in a grid-like structure, with teams positioning themselves at varying distances from the swarm's centroid at steady state. Our findings confirmed this hypothesis: applying SVO as a weight to the coordinate coupling matrix that governs the repulsive force among agents leads to the emergence of a grid-like structure. At steady state, teams with different SVO values arrange themselves at distinct distances from the centroid, highlighting the influence of SVO on the spatial distribution of agents within the swarm.

In addition to investigating spatial distribution, we also analyzed the impact of SVO on the rotational dynamics of the agents. The rotational behavior of the swarm was examined by varying the SVO value for a single agent while keeping the SVO values of other agents constant. Frequency analysis of the agents' rotational speeds revealed that increasing SVO primarily shifts the dominant low-frequency component towards higher frequencies. This suggests that higher SVO values induce jittery rotational behavior in the affected agent and faster speed, while the overall motion remains smooth and dominated by low frequencies. The results indicate that the influence of SVO on rotational dynamics is localized, primarily affecting the agent with the varying SVO, while other agents maintain stable rotational

motion regardless of the changes in SVO.

3.1 Problem Formulation

Consider a swarm of N agents, where the position of each agent at time $t \geq 0$ is denoted by $\mathbf{z}_i(t) \in \mathbb{R}^d$, $i = 1, 2, \ldots, N$, with $d = 3$ for the three-dimensional space. The dynamic model for the position of each agent is described by a single integrator as follows:

$$\dot{\mathbf{z}}_i(t) = \mathbf{u}_i(t), \quad i = 1, 2, \ldots, N \tag{3.1}$$

where $\mathbf{u}_i(t) \in \mathbb{R}^d$ represents the control input for agent i. The control protocol is designed to achieve two goals: 1. Ensure the agents aggregate in a bounded region around the centroid of the swarm. 2. Depending on the simulation scenario either influence the relative distance of the agents to the centroid based on their assigned SVO or influence the rotational speed of the agents based on their assigned SVO.

The centroid of the swarm is given by:

$$\mathbf{z}_c(t) = \frac{1}{N} \sum_{i=1}^{N} \mathbf{z}_i(t) \tag{3.2}$$

The agents interact through both attractive and repulsive forces, where the attractive force encourages aggregation towards the centroid, and the repulsive force ensures agents maintain some distance from each other.

3.1.1 Interaction Model

The control input $\mathbf{u}_i(t)$ for each agent is based on the interactions with its neighbors and is defined as:

$$\mathbf{u}_i(t) = \sum_{j \neq i} (-g_{\text{att}}(\mathbf{z}_i(t) - \mathbf{z}_j(t)) * H * (\mathbf{z}_i(t) - \mathbf{z}_j(t)) + g_{\text{rep}}(\mathbf{z}_i(t) - \mathbf{z}_j(t)) * M * (\mathbf{z}_i(t) - \mathbf{z}_j(t)) \tag{3.3}$$

where g_{att} represents the attractive force, and g_{rep} represents the repulsive force H and M are coordinate coupling matrices. SVO values are defined in the coordinate coupling matrices separately. Table 3.1 shows how each parameter change in the scenarios.

Table 3.1: Summary of Parameters for Each Scenario

Scenario	$g_{\text{att}}(\mathbf{y})$	$g_{\text{rep}}(\mathbf{y})$	H	M
1st Scenario	1	$\frac{1}{\|\mathbf{y}\|}$	$\frac{1}{\xi_i} \cdot \mathbf{I}_{3\times3}$	$\begin{bmatrix} 1 & 0 & 0 \\ 0 & 0 & 0 \\ 0 & 0 & 1 \end{bmatrix}$
2nd Scenario	1	$\frac{1}{\|\mathbf{y}\|^2}$	$\mathbf{I}_{3\times3}$	$\xi_i \cdot \begin{bmatrix} 1 & 0 & 0 \\ 0 & 0 & 0 \\ 0 & 0 & 1 \end{bmatrix}$
3rd Scenario	N	0	$\xi_i \cdot \begin{bmatrix} 0 & -w_z & w_y \\ w_z & 0 & -w_x \\ -w_y & w_x & 0 \end{bmatrix}$	0

The first two scenarios focus on simulating spatial arrangements, while the third scenario examines differences in rotational behavior. Table 3.1 summarizes the parameters for each case. In the first scenario, the attraction force is linearly changing due to the inter-agent distance, the repulsion force is constant when multiplied with the distance vector between agents, and the SVO parameter is inversely proportional to the coordinate coupling matrix associated with the attraction force. In the second scenario, the attraction force remains the same as in the first scenario, but the repulsion force becomes unbounded, and the SVO parameter is applied to the coordinate coupling matrix related to the repulsion force.

In the third scenario, the attraction force is proportional to the number of agents in the simulation and is again linearly changing. There is no repulsion force in this case, and the SVO parameter modulates the coordinate coupling matrix, which governs the rotational behavior. The parameters w_x, w_y, and w_z are set to 1, -2, and 3, respectively. For further details on how these parameters are selected, refer to Fedele et al. [2022].

3.1.2 Graph Representation of Swarm

We assume that, a swarm of N agents is modeled as a graph $G = (V, E)$, where the agents are represented as the nodes of the graph, and the interactions between agents, which arise from sensing and communication, are represented as the edges of the graph. Specifically,

for each pair of agents i and j, an edge (i, j) exists in the graph if agent i can sense or communicate with agent j.

In this model, we assume that every agent can sense and communicate with every other agent in the swarm. As a result, the graph G is complete, meaning that there is an edge between every pair of nodes in the graph. This complete graph structure implies that the interactions between agents are global, as each agent has direct access to the position and state information of every other agent in the swarm. The complete nature of the graph ensures that all agents contribute to the overall swarm behavior through their interactions, regardless of their relative distance or positioning.

3.2 Influence of SVO on Swarm's Spatial Arrangement

The simulation model aims to study the effects of SVO on the spatial distribution of agents in a multi-agent system. Agents are grouped into teams, each assigned a different SVO value, and their positions in space are analyzed to observe the influence of SVO on their distances to the swarm's centroid. The simulation operates in a 3D space where agents interact through repulsive and attractive forces, and SVO is used as a weight to modify the forces among agents.

3.2.1 First Example

The simulation involves a swarm of $N = 144$ agents, divided into 10 teams. Each team is assigned a unique SVO value from 0.1 to 1.0. The sizes of the teams vary, with larger teams assigned to more cooperative agents. The specific sizes of the teams are as follows:

$$\text{Team Sizes: } [3, 5, 7, 9, 12, 15, 18, 20, 25, 30]$$

The SVO values assigned to each team range from 0.1 to 1.0, incremented equally across the teams:

$$\text{SVO Values: } [0.1, 0.2, 0.3, \ldots, 1.0]$$

Larger teams exhibit a stronger repulsive force, which leads them to position themselves farther from the swarm's centroid.

3.2.1.1 Attractive Force

The attractive component is defined by the term $-g_{\text{att}}(\mathbf{z}_i(t) - \mathbf{z}_j(t)) * H_i * (\mathbf{z}_i(t) - \mathbf{z}_j(t))$ in equation 3.3. From now on we use $\mathbf{z}_i(t) - \mathbf{z}_j(t)$ and $\mathbf{y}$ interchangebly:

- $g_{\text{att}}(\mathbf{y})$ is a function that determines the strength of the attractive force based on the distance between agents. It is designed to take the inter-agent distance as a parameter however in this case it is constant so when paired with the inter-agent distance vector, it changes linearly due to the distance between agents.
- H_i is a matrix that governs the direction and magnitude of the attractive force, with H_i set as $\frac{1}{\xi_i} \cdot \mathbf{I}_{3\times3}$. That way, we include SVO into the attraction force, with smaller SVO attraction force becomes larger therefore agents pull themselves towards the center more aggresively.

Scaling H_i by the SVO value of agent i results in a grid-like pattern where agents with smaller SVO values exhibit stronger attractive forces, reducing the distance to the centroid of the swarm.

3.2.1.2 Repulsive Force

The repulsive component is defined by the term $g_{\text{rep}}(\mathbf{y})M\mathbf{y}$, where:

- $g_{\text{rep}}(\mathbf{y})$ is a function that determines the strength of the repulsive force based on the distance between agents. It is selected to be $\frac{1}{||y||}$ so the repulsion force is constant when paired with the inter-agent distance vector.
- M is a diagonal matrix that produces one zero eigenvalue. So forces along that direction becomes zero, resulting with agents aggregating in a 2D plane.

The matrix M is constructed as:

$$M = \begin{bmatrix} 1 & 0 & 0 \\ 0 & 0 & 0 \\ 0 & 0 & 1 \end{bmatrix}$$

This formulation implies that the repulsive force acts primarily in the x- and z-directions. The matrix M is designed to have two orthogonal eigenvalues and one zero eigenvalue. Specifically, the eigenvalues are $\lambda_1 = 1$, $\lambda_2 = 1$, and $\lambda_3 = 0$, corresponding to the x-, z-, and y-directions, respectively. This configuration ensures that the agents' motion is constrained to a 2D plane (the x-z plane) at steady state, while there is no repulsive force in the y-direction.

Moreover, if the two positive eigenvalues are identical (i.e., $\lambda_1 = \lambda_3 = 1$), the agents will position themselves in a circular pattern on the plane. However, if the eigenvalues are set to different values (e.g., $\lambda_1 = 2$ and $\lambda_3 = 1$), the agents will form an elliptical configuration at steady state, with the aspect ratio of the ellipse determined by the ratio of the eigenvalues. This flexibility allows the matrix M to control the shape of the agents' spatial arrangement while maintaining repulsive interactions primarily in the x- and z-directions.

3.2.1.3 Simulation Results and Discussion

In this section, we present and analyze the results of the simulation. The simulation was designed to explore how different SVO values affect the spatial distribution of agents within a swarm. Specifically, we hypothesized that teams with higher SVO values would position themselves further from the swarm centroid, forming a grid-like or concentric structure around the center. Below, we discuss the outcomes of two key visualizations of the simulation.

Figure 3.1 shows the final positions of agents, with each team colored according to their SVO value. The agents are plotted in three-dimensional space, where the x-axis represents the X-position, the y-axis represents the Y-position, and the z-axis represents the Z-position. Each team is represented by a distinct color, as shown in the legend, which corresponds to the team's SVO value.

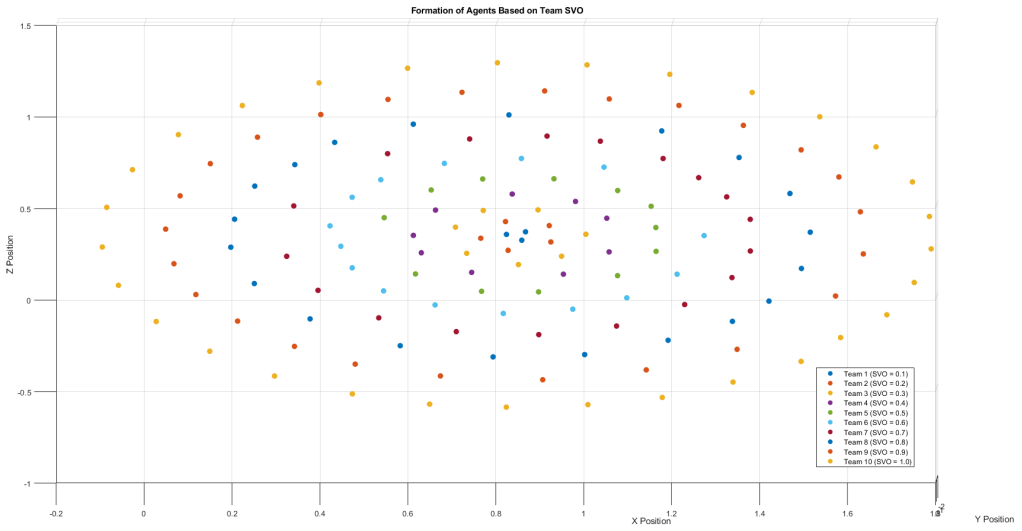

Figure 3.1: Formation of agents based on their team SVO values. Teams with higher SVO values position themselves farther from the center of the swarm.

As seen in Figure 3.1, teams with lower SVO values (e.g., Team 1, SVO = 0.1, represented in blue) are positioned closer to the center of the swarm, while teams with higher SVO values (e.g., Team 10, SVO = 1.0, represented in yellow) occupy positions further from the center. This visual distribution clearly supports the hypothesis that lower SVO values increase the attractive forces experienced by the agents, causing them to position themselves closer to the centroid.

This behavior confirms that the inclusion of SVO in the coordinate coupling matrices significantly influences the spatial distribution of agents. Lower SVO values correspond to a stronger attractive force, pulling those agents closer to the centroid and leading to the observed concentric structure.

Figure 3.2 presents a bar chart showing the average distance of agents from the centroid, calculated for each team. The x-axis represents the SVO values assigned to each team, while the y-axis represents the average distance from the swarm's center of mass.

As seen in Figure 3.2, the results show a clear increasing trend, where higher SVO values are associated with larger average distances to the center. For example, agents with an SVO of 0.1 have a very small average distance to the center, while agents with an SVO of 1.0 have the largest average distance. This trend quantitatively confirms the observation from Figure 3.1: agents with lower SVO values are pulled closer to the centroid due to the

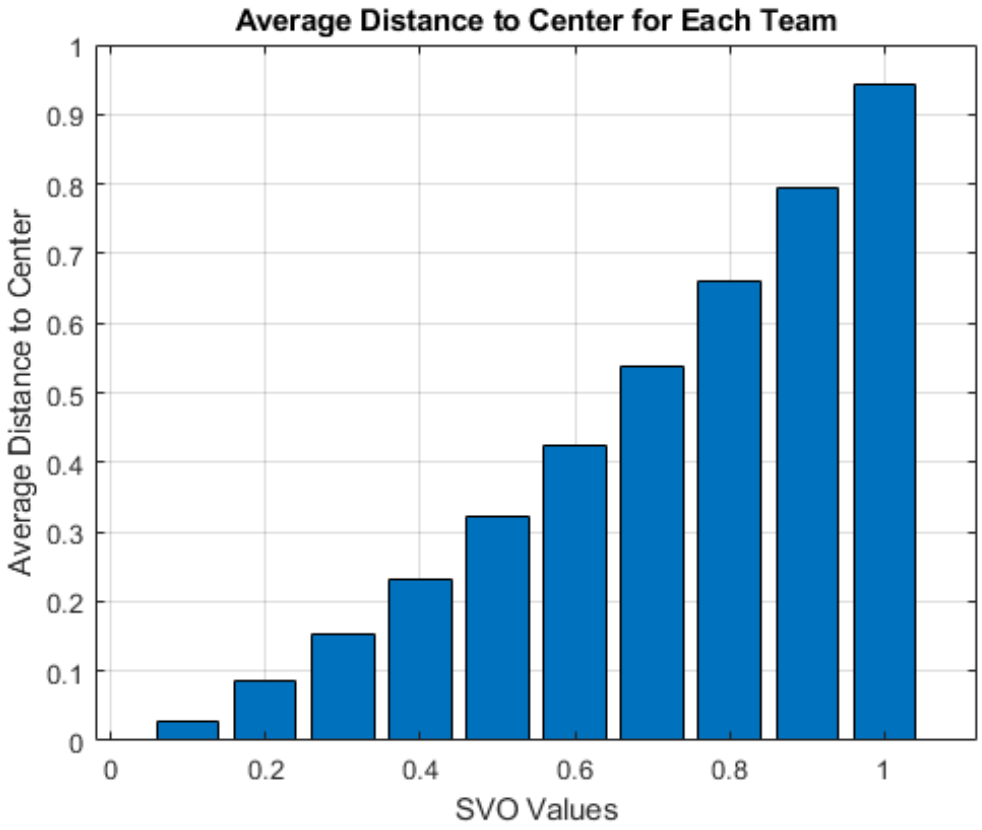

Figure 3.2: Average distance to the center for each team. As the SVO value increases, the average distance to the center of the swarm increases as well.

stronger attractive forces associated with those values.

The clear linear progression between SVO values and average distances further supports the conclusion that SVO directly modulates the spatial configuration of the swarm. The attractive forces, which are weighted by the SVO parameter, act more strongly on agents with higher SVO values, leading them to maintain a closer formation to the centroid. As a result, teams with higher SVO values form the outer layers of the swarm, while teams with lower SVO values cluster closer to the center.

Furthermore, we created three metrics to ensure that the observed outcomes are not coincidental. The same simulations were repeated 30 times with randomized initial positions. The three metrics are described as follows:

1. Initial vs. Final Average Distances: This metric calculates the average distance of all agents to the center of the swarm, both at the beginning and at the end of the simulation.

It provides a general measure of how the system is clustered around the center.

2. Mean Squared Error (MSE) of Distances: This metric is defined as:

$$MSE = \sqrt{\frac{1}{N}\sum_{i=1}^{N}(d_i - \overline{d})^2} \tag{3.4}$$

where d_i represents the distance of the i-th agent to the center, and $\overline{d}$ is the average distance of all agents to the center. The MSE quantifies the variability in distances among the agents.

3. Range of Distances: This metric determines the spread of the agents by calculating the difference between the maximum (d_{max}) and minimum (d_{min}) distances:

$$d_{range} = d_{\text{max}} - d_{\text{min}} \tag{3.5}$$

This value represents how widely the agents are distributed across the simulation area.

The overall average distance indicates the extent to which the system is generally clustered around the center. The mean squared error reflects the variability in distances among agents, while the range of distances measures the spatial spread of the system. Below, the results of the three metrics are visualized in Figures 3.3, 3.4, and 3.5.

The two visualizations presented in Figures 3.1 and 3.2 together demonstrate the critical role of SVO in shaping the spatial distribution of agents within the swarm. The three-dimensional scatter plot in Figure 3.1 visually illustrates how teams with higher SVO values occupy positions further from the centroid, forming a grid-like or concentric structure. The bar chart in Figure 3.2 quantitatively confirms this observation, showing a clear relationship between higher SVO values and greater average distances from the center.These results validate the hypothesis that introducing SVO into the interaction dynamics of agents influences their spatial behavior.

As shown in Figures 3.3, 3.4, and 3.5, the results indicate that, even though it is not analytically proven, agents tend to exhibit similar behaviors under similar circumstances, even when initialized with randomized positions. This iterative verification serves as a foundation for future analytical work, providing empirical evidence to support the observed patterns.

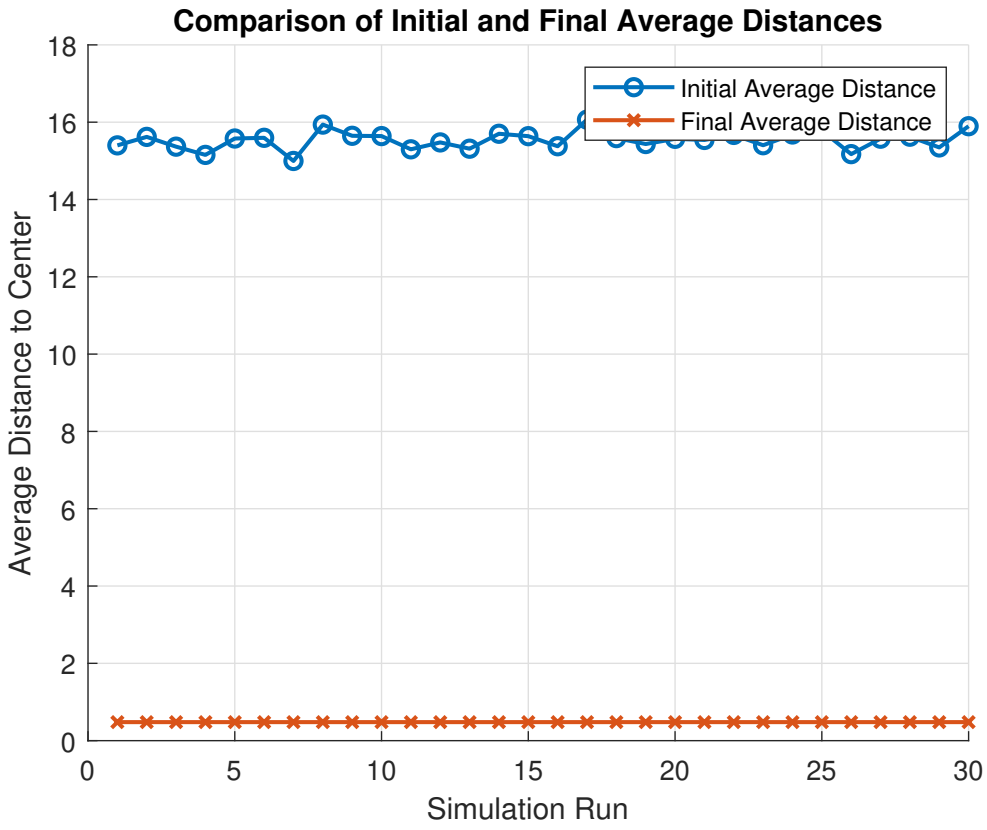

Figure 3.3: Comparison of initial and final average distances of agents to the center.

These findings suggest that the system's dynamics are robust to variations in initial conditions, demonstrating consistency in the agents' behavior across multiple trials. This consistency reinforces the validity of the simulation model and highlights its potential for developing analytical frameworks in future research.

3.2.2 Second Example

The second simulation shares the same setup as the first one. However, in this case, the repulsion force is defined differently, and the modulation of SVO is applied to the coordinate coupling matrix affecting the repulsion term. The differences are explained below.

3.2.2.1 Repulsive Force

The repulsive component is defined by the term $g_{\text{rep}}(\mathbf{y})M_i\mathbf{y}$, where:

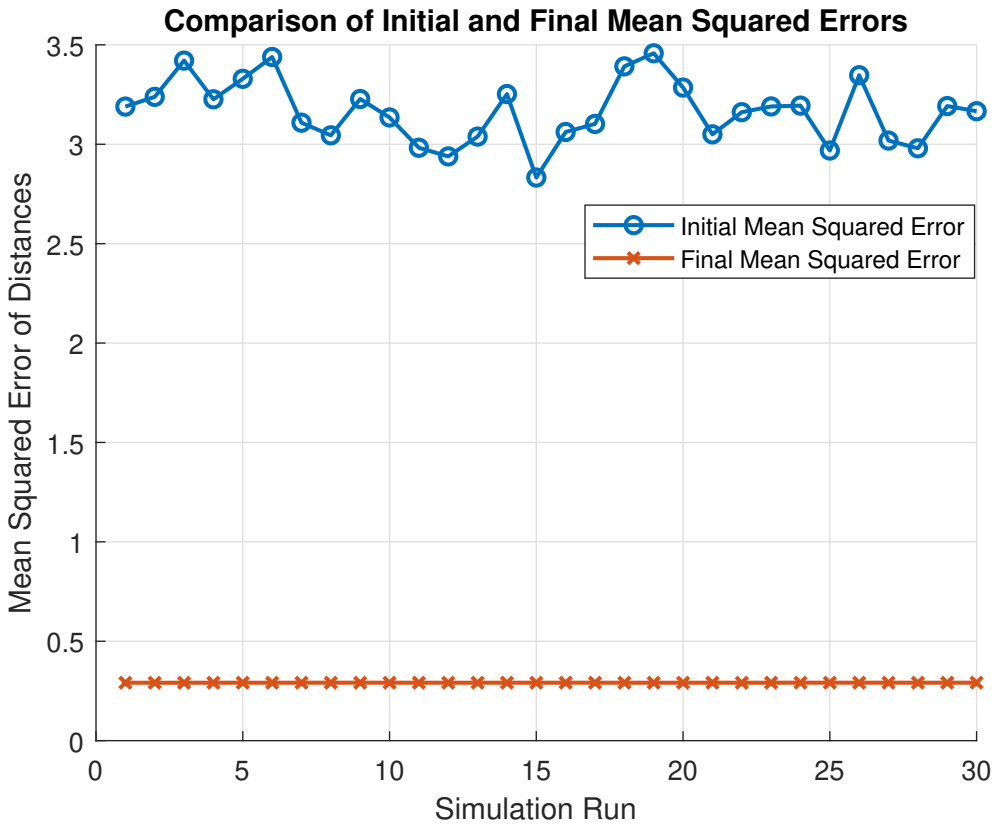

Figure 3.4: Mean squared error of distances between agents and the center.

- $g_{\text{rep}}(\mathbf{y})$ is a function that determines the strength of the repulsive force based on the distance between agents. It is selected as $\frac{1}{\|\mathbf{y}\|^2}$, making the repulsion force unbounded as agents get closer.

- M_i is a diagonal matrix that includes one zero eigenvalue, causing forces along that direction to vanish. This ensures that agents push each other only in a 2D plane. With M_i set as $\xi_i \cdot M$, the SVO parameter modulates the repulsion force. Agents with larger SVO values exert stronger repulsion, pushing themselves away from each other more aggressively.

The attraction matrix H is a 3×3 identity matrix, and the matrix M is constructed as:

$$M_i = \xi_i \begin{bmatrix} 1 & 0 & 0 \\ 0 & 0 & 0 \\ 0 & 0 & 1 \end{bmatrix}$$

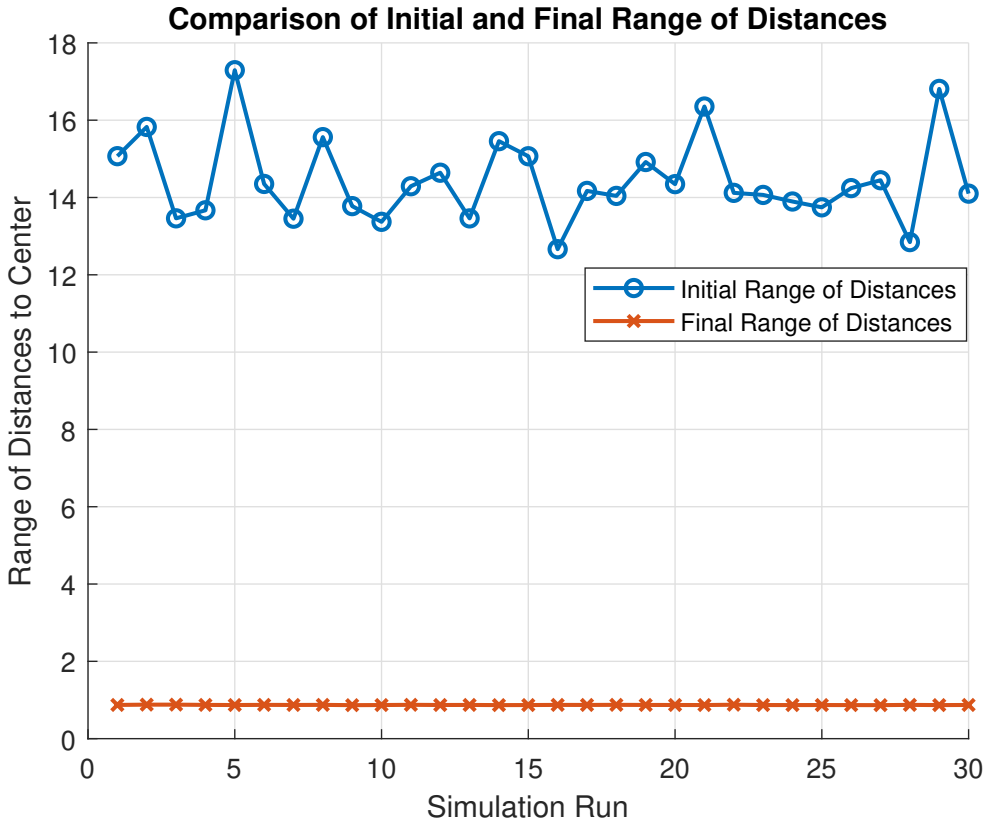

Figure 3.5: Range of distances (difference between maximum and minimum distances of agents).

3.2.2.2 Simulation Results and Discussion

Here, we present and analyze the results of the simulation. Similar to the first example, the simulation explores how different SVO values affect the spatial distribution of agents within the swarm. We hypothesized again that teams with higher SVO values would position themselves farther from the swarm centroid, forming a grid-like structure around the center. However, in this case, the modulation of SVO is applied to the repulsion force instead of the attraction force. While SVO was applied inversely proportional in the first simulation, here it is applied directly.

Figure 3.6 shows the final positions of agents, with each team colored according to their SVO value. The agents are plotted in three-dimensional space, where the x-axis represents the X-position, the y-axis represents the Y-position, and the z-axis represents the

Z-position. Each team is represented by a distinct color, as shown in the legend, which corresponds to the team's SVO value.

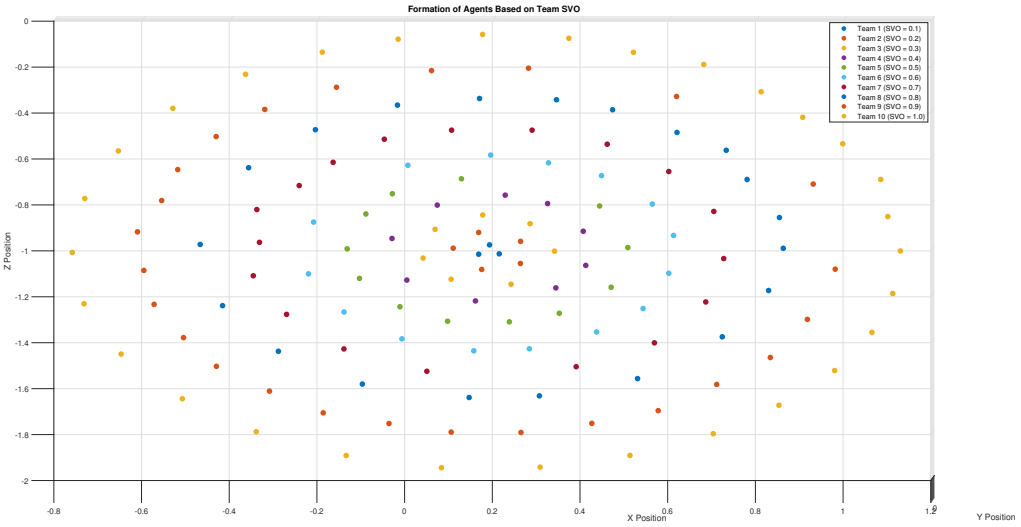

Figure 3.6: Formation of agents based on their team SVO values. Teams with higher SVO values position themselves farther from the center of the swarm.

As seen in Figure 3.6, teams with lower SVO values are positioned closer to the center of the swarm, while teams with higher SVO values occupy positions farther from the center. Notably, whether the difference among agents is created using the attraction force or the repulsion force, the grid-like structure is still achieved. This visual distribution supports the hypothesis that higher SVO values increase the repulsive forces experienced by the agents, causing them to position themselves farther from the centroid.

Figure 3.7 presents a bar chart, similar to the first example, showing the average distance of agents from the centroid, calculated for each team. The x-axis represents the SVO values assigned to each team, while the y-axis represents the average distance from the swarm's center of mass.

The clear linear progression between SVO values and average distances once again supports the conclusion that SVO directly modulates the spatial configuration of the swarm.

To ensure that the observed outcomes are not coincidental, we used the same three metrics as in the first example. The same simulations were repeated 30 times with randomized initial positions. The results of the three metrics are shown below.

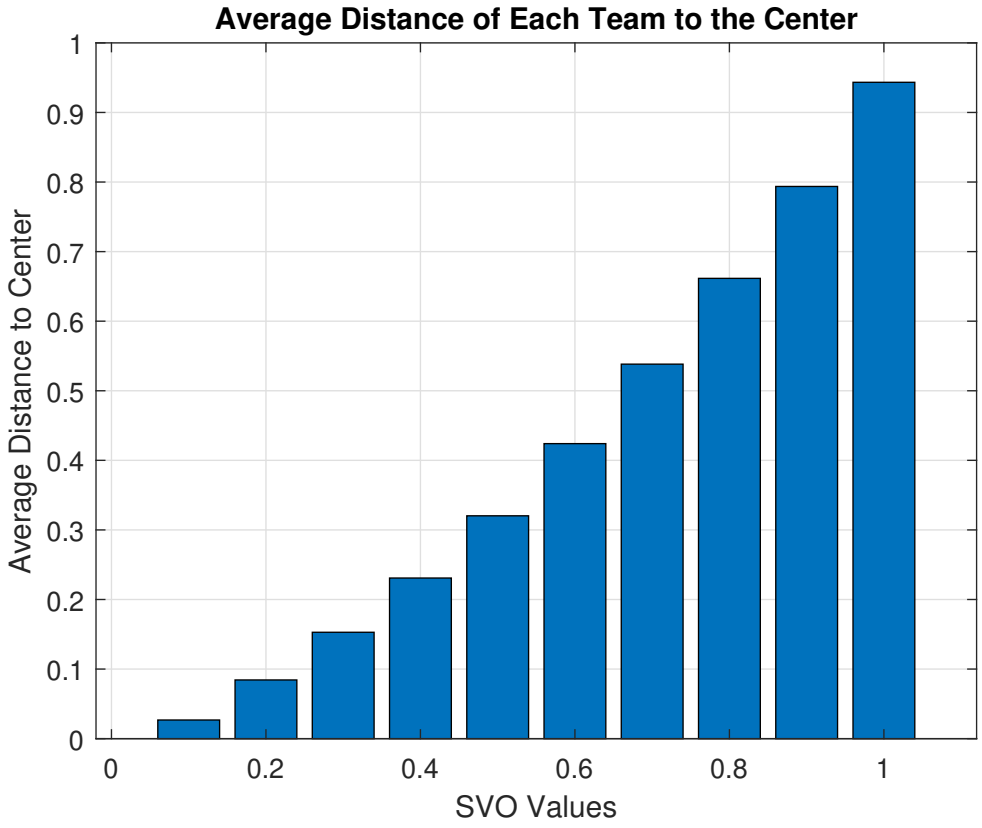

Figure 3.7: Average distance to the center for each team. As the SVO value increases, the average distance to the center of the swarm increases as well.

The visualizations presented in Figures 3.6 and 3.7 demonstrate the critical role of SVO in shaping the spatial distribution of agents within the swarm. The three-dimensional scatter plot in Figure 3.6 visually illustrates how teams with higher SVO values occupy positions farther from the centroid due to increased repulsion, forming a grid-like structure. The bar chart in Figure 3.7 quantitatively confirms this observation, showing a clear relationship between higher SVO values and greater average distances from the center.

As in the first example, the results indicate that agents tend to exhibit similar behaviors under similar circumstances when initialized with randomized positions. These findings suggest that SVO is a versatile parameter that can be applied in different aspects of the system's dynamics, allowing for flexible modulation of swarm behavior.

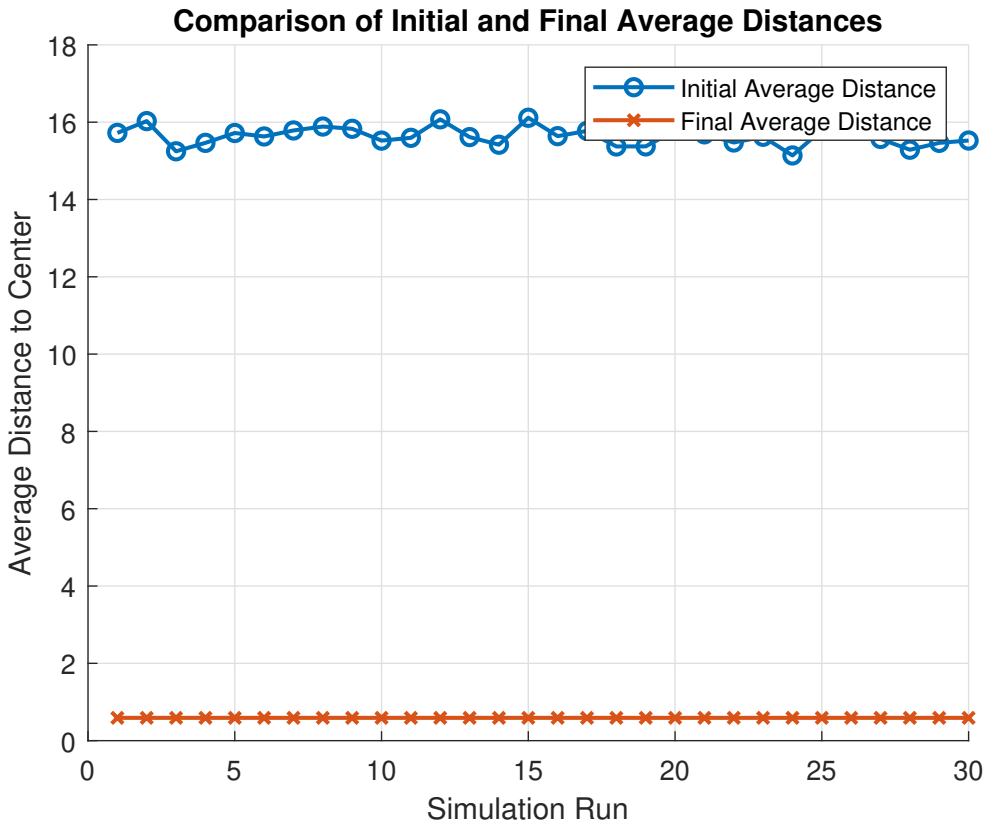

Figure 3.8: Comparison of initial and final average distances of agents to the center.

3.3 Influence of SVO on Swarm's Rotational Behavior

3.3.1 Rotational Behavior Through Skew-Symmetric Matrices

To achieve rotational behavior in a swarm, we employ the approach introduced in Fedele et al. [2022], which extends the Gazi-Passino model by incorporating coordinate-coupling matrices. In this context, a skew-symmetric matrix is used to induce rotational motion around a designated axis. Here, we explain how a skew-symmetric matrix generates such rotational behavior and how coupling it with the SVO parameter influences the rotational speed.

A matrix H is defined as skew-symmetric if it satisfies the condition:

$$H = -H^T$$

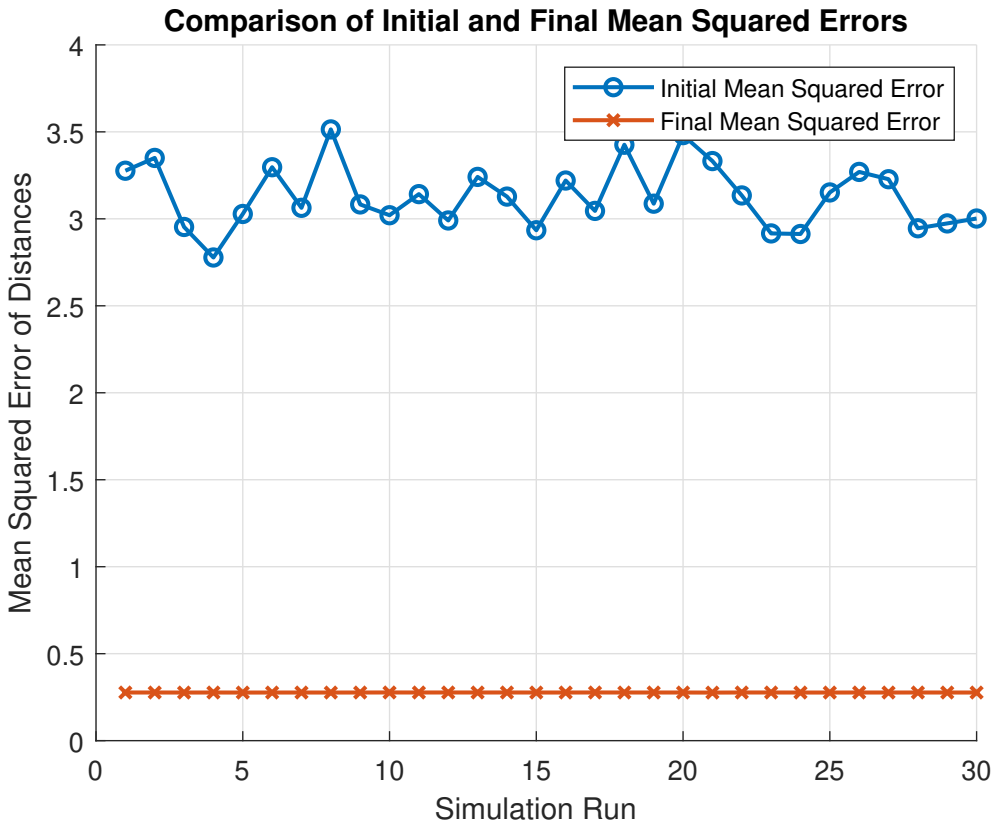

Figure 3.9: Mean squared error of distances between agents and the center.

where H^T is the transpose of H. In a three-dimensional space, the skew-symmetric matrix can be expressed as:

$$H = \begin{bmatrix} 0 & -w_z & w_y \\ w_z & 0 & -w_x \\ -w_y & w_x & 0 \end{bmatrix}$$

where w_x, w_y, and w_z are components that define the rotation axis. This matrix effectively represents the cross-product operation with a vector $\mathbf{w} = [w_x, w_y, w_z]^T$, which can be interpreted as the angular velocity vector.

The skew-symmetric matrix H induces rotational behavior by generating velocities or forces that are perpendicular to the current position vector of the agents. When applied to a position vector $\mathbf{y}$, the resulting vector $\mathbf{v} = H\mathbf{y}$ is always orthogonal to $\mathbf{y}$, satisfying the condition:

$$\mathbf{v} \cdot \mathbf{y} = 0$$

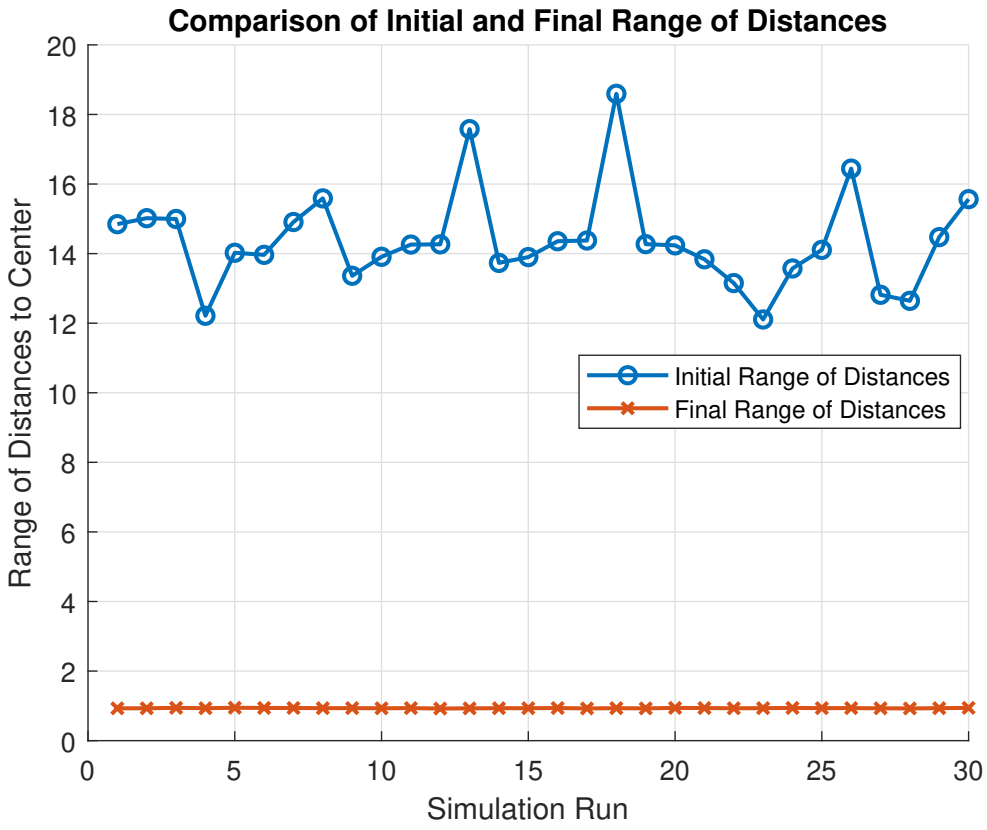

Figure 3.10: Range of distances (difference between maximum and minimum distances of agents).

This orthogonality ensures that the motion is confined to a circular path around the rotation axis defined by $\mathbf{w}$. As such, the skew-symmetric matrix creates rotational trajectories, guiding agents to follow curved paths around the swarm's centroid while maintaining a specified rotational frame.

3.3.2 Coupling Skew-Symmetric Matrices with SVO

In our model, we extend the work of Fedele et al. [2022] by incorporating the SVO parameter into the skew-symmetric matrix to modulate the rotational speed of each agent.

Specifically, we define the modified skew-symmetric matrix for the i-th agent as:

$$H_i = \xi_i \cdot \begin{bmatrix} 0 & -w_z & w_y \\ w_z & 0 & -w_x \\ -w_y & w_x & 0 \end{bmatrix}$$

where ξ_i represents the SVO of the i-th agent. By scaling the skew-symmetric matrix with ξ_i, we adjust the rotational velocity for each agent individually. As the SVO value increases, the magnitude of the resulting rotational force also increases, thereby enhancing the rotational speed around the designated axis.

This coupling allows us to introduce variability in the agents' rotational behavior, directly linking the SVO parameter to the dynamics of the swarm. Higher SVO values lead to faster rotation rates, as the scaling effect amplifies the influence of the angular velocity vector **w**. This mechanism provides a way to control not only the spatial arrangement of agents but also their rotational dynamics, offering a flexible approach to modulating swarm behaviors.

3.3.3 Third Example

In this section, we analyze the effect of SVO on the frequency spectrum of the agents' motion. A series of simulations were conducted where the SVO value for the tenth agent was varied across a range of values from 0.1 to 1.0, while the remaining agents had a constant SVO of 0.1. The aim of this analysis is to understand the impact of SVO variations on the overall movement dynamics, specifically in terms of the frequency components of the agents' positional behavior over time. This simulation contains $N = 10$ agents.

The frequency spectra for each agent, across all SVO values, exhibit a common pattern: the motion of all agents is primarily dominated by low-frequency components, with the most significant peaks appearing below 5 Hz. This suggests that the agents' movements are smooth and steady, with no abrupt or high-frequency oscillations. The low-frequency peaks indicate that the agents' positions oscillate gently over time, consistent with the objective of maintaining a cohesive and stable swarm.

The tenth agent, whose SVO was varied across simulations, displayed distinct behavior compared to the other agents. As shown in the superposed frequency spectra in Figure 3.11, the dominant peaks for Agent 10 shift and increase in magnitude as the SVO value increases from 0.1 to 1.0. This trend indicates that higher SVO values amplify the agent's motion, leading to more pronounced oscillations. Specifically, the magnitude of the primary low-frequency peak increases with the SVO value, reflecting a greater extent of movement and more dynamic behavior. This behavior suggests that Agent 10's motion becomes increasingly energetic as its SVO value increases, though the motion remains primarily within the low-frequency range.

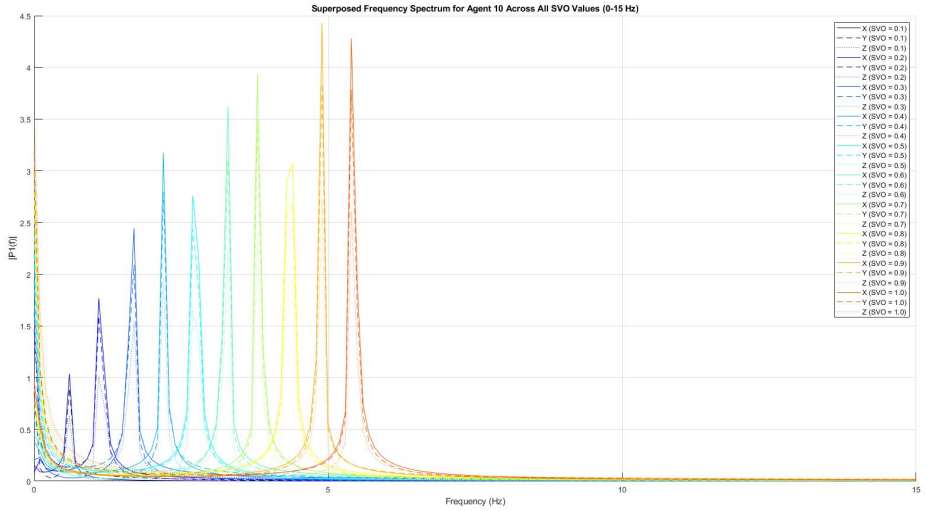

Figure 3.11: Superposed Frequency Spectrum for Agent 10 Across All SVO Values (0-15 Hz). The plot shows the variation in frequency components as the SVO value increases, with distinct peaks indicating changes in motion dynamics.

Notably, for higher SVO values (SVO ≥ 0.7), the frequency spectrum shows additional peaks or slight broadening around the dominant low-frequency range. While these higher-frequency components are relatively minor, they indicate that higher SVO values introduce subtle complexity into the agent's motion. This could imply that Agent 10 experiences slightly more variable movement patterns or deviations from strictly periodic behavior at higher SVO levels. However, these components are insignificant compared to the dominant low-frequency peaks, indicating that the overall motion remains smooth and predominantly low-frequency.

The frequency spectra for Agents 1 to 9 show minimal changes across the SVO iterations. Their motion remains dominated by the same low-frequency oscillations, with no significant variations in frequency magnitude or the emergence of higher-frequency components. This stability confirms that the SVO variations applied to Agent 10 have a localized effect, influencing only the behavior of that specific agent while the others maintain their stable, predictable movement patterns. The unchanged behavior of these agents supports the conclusion that the effects of SVO on an individual agent do not propagate through the swarm under the simulation conditions.

Also we can see the trajectories of all agents for the first iteration. We see that they rotate around a fixed axis and have slight deviations from their trajectories so they form a disk rather than a perfect circle.

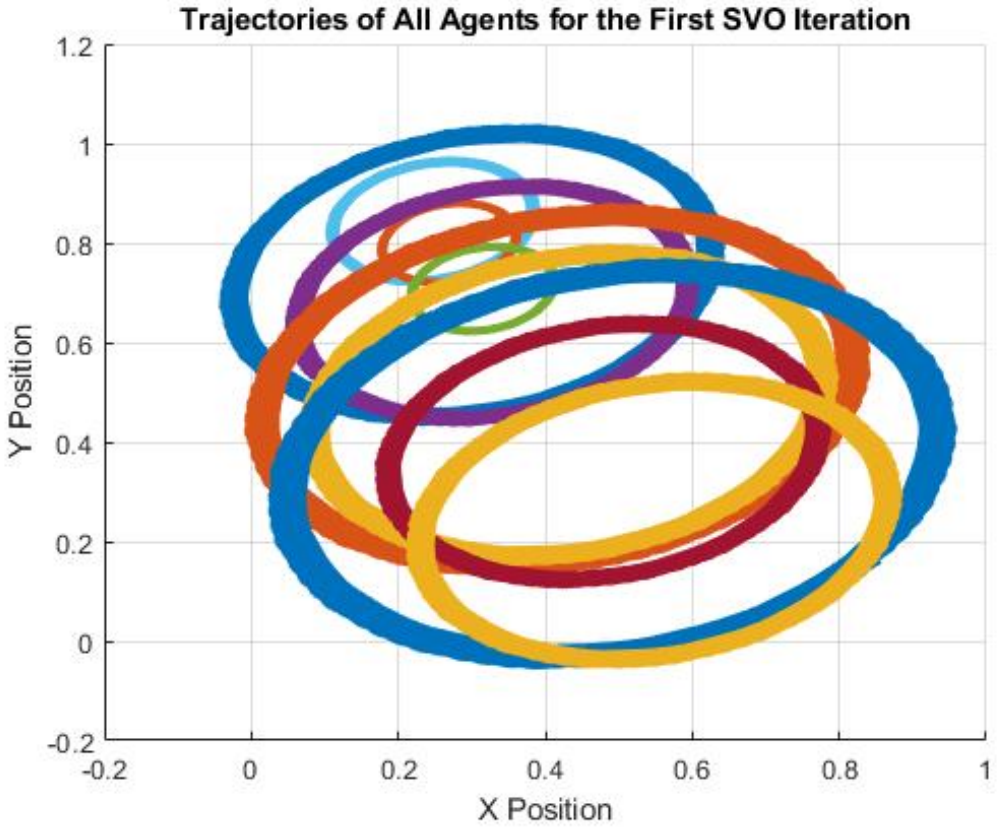

Figure 3.12: Trajectories of all agents for the first iteration.

3.3.4 Conclusion on Frequency Analysis

The frequency analysis reveals that the primary effect of SVO variation is a change in the magnitude and sharpness of the low-frequency components for Agent 10. As the SVO value increases, Agent 10 exhibits a more dynamic behavior, reflected in the increasing magnitude of its dominant frequency peak. The appearance of slight higher-frequency elements at higher SVO values further suggests that increasing SVO can introduce subtle variability into the agent's movement patterns, although these remain secondary to the dominant low-frequency oscillations.

The other agents remain unaffected by the change in SVO for Agent 10, consistently displaying stable low-frequency motion throughout all simulations. This indicates that, under the given conditions, the impact of SVO on an individual agent's motion is localized and does not influence the behavior of the entire swarm.

4. CONCLUSION

This dissertation investigates the role of *behavioral heterogeneity*, also termed *mild heterogeneity*, in multi-agent systems by integrating SVO into each agent's control law. Mild heterogeneity refers to variations in agent parameters while preserving the same overarching dynamics, thus allowing agents to exhibit diverse behavioral traits within a unified framework. By bridging concepts from social psychology and control theory, this study offers new insights into how individual behaviors collectively shape swarm performance, shedding light on both the theoretical underpinnings and practical applications of heterogeneous agent interactions.

The key contributions can be summarized as follows. The first part of this work focuses on a target-capturing problem, where agents converge to an ellipsoidal "containment region" around a stationary target without intruding on a smaller "distancing region." Prior analyses had shown that under certain boundary conditions, agents complete this task in finite time. Building on this, we prove that introducing SVO does not undermine existing convergence guarantees: selfish agents (low SVO) reach the target more rapidly, while prosocial agents (high SVO) emphasize group cohesion at the expense of slower convergence. Despite these behavioral differences, the system retains its overall stability and ensures that each agent settles into the containment region without violating the distancing constraint.

The second part of the dissertation investigates formation control and rotational dynamics through the incorporation of SVO into attraction-repulsion functions and coordinate coupling matrices. Two main simulation scenarios illustrate the influence of SVO on steady-state formations and angular velocities. In the first scenario, agents grouped by similar SVO values self-organize into grid-like or concentric-layer formations, a phenomenon consistently replicated under varied initial conditions. Fourier Transform analysis in the

second scenario demonstrates that SVO variations significantly increase the dynamic complexity of agent motion, with higher frequency components evident, revealing a strong link to SVO settings and collective movement patterns.

These contributions highlight that SVO can serve as an effective tool for introducing behavioral heterogeneity without sacrificing key properties like convergence and collision avoidance. By balancing individual performance and group cohesion, SVO-driven approaches broaden the applicability of swarm models to more nuanced, real-world tasks.

From a theoretical perspective, this dissertation demonstrates how mild heterogeneity can be seamlessly integrated into existing control frameworks. These findings show that heterogeneous swarms can retain core stability properties while exhibiting richly varied behaviors. This opens avenues for studying emergent dynamics where individual-level variations lead to collective outcomes that may be more adaptable or robust.

From a practical standpoint, the insights gained here have direct relevance for domains such as robotics, autonomous vehicles, and distributed decision-making. By tuning SVO parameters, practitioners can tailor agent behaviors to prioritize either rapid task completion, tight formation, or any balance in between. Such flexibility is crucial in applications ranging from search-and-rescue missions—where swift action is paramount—to long-duration surveillance tasks requiring stable, cohesive group structures.

Several limitations and open questions pave the way for future investigations: The majority of this study assumes a connected or complete interaction topology. Exploring how SVO-based heterogeneity functions under time-varying or partially connected networks remains an important area of inquiry.

Although simulations strongly support the efficacy of SVO-driven control, and some bounded error is included theoretically, implementing these methods on physical platforms would uncover practical constraints such as sensor noise, communication delays, and unpredictable disturbances.

This dissertation focuses on cooperative scenarios with shared objectives. Extending SVO to competitive or adversarial contexts could yield insights into resource allocation, conflict resolution, or game-theoretic strategies within heterogeneous swarms.

In conclusion, this dissertation establishes SVO as a powerful mechanism for embedding

behavioral heterogeneity into multi-agent systems, demonstrating that it can be done without undermining convergence or stability. From target-capturing under quadcopter dynamics to more general formation and rotational behaviors, the results confirm that SVO significantly enriches the behavioral spectrum of swarms. This enriched diversity provides fertile ground for both fundamental research on emergent dynamics and practical applications in complex, real-world tasks. Future directions include more analytical work for the missing parts, validating these methods in physical testbeds, extending SVO to competitive environments, and integrating it with sophisticated control or machine learning frameworks. As research continues, embracing behavioral heterogeneity promises to foster more resilient, efficient, and intelligent multi-agent systems, ultimately expanding the frontiers of swarm coordination and control.

BIBLIOGRAPHY

T. Baca, M. Petrlik, M. Vrba, V. Spurny, R. Penicka, D. Hert, and M. Saska. The mrs uav system: Pushing the frontiers of reproducible research, real-world deployment, and education with autonomous unmanned aerial vehicles. *Journal of Intelligent and Robotic Systems*, 102(1):1–28, 2021.

Guangyan Bao, Lifeng Ma, and Xiaojian Yi. Recent advances on cooperative control of heterogeneous multi-agent systems subject to constraints: A survey. *Systems Science & Control Engineering*, 10(1):539–551, 2022.

László Blázovics, Tamás Lukovszki, and Bertalan Forstner. Target surrounding solution for swarm robots. In *Meeting of the European Network of Universities and Companies in Information and Communication Engineering*, pages 251–262. Springer, 2012.

Antonio Bono, Luigi D'Alfonso, Giuseppe Fedele, and Veysel Gazi. Target capturing in an ellipsoidal region for a swarm of double integrator agents. *IEEE/CAA Journal of Automatica Sinica*, 9(5):801–811, 2022.

Noam Buckman, Alyssa Pierson, Wilko Schwarting, Sertac Karaman, and Daniela Rus. Sharing is caring: Socially-compliant autonomous intersection negotiation. In *2019 IEEE/RSJ International Conference on Intelligent Robots and Systems (IROS)*, pages 6136–6143, 2019. doi: 10.1109/IROS40897.2019.8967997.

Yongcan Cao, Daniel Stuart, Wei Ren, and Ziyang Meng. Distributed containment control for multiple autonomous vehicles with double-integrator dynamics: algorithms and experiments. *IEEE Transactions on Control Systems Technology*, 19(4):929–938, 2010.

Tianguang Chu, Long Wang, and Tongwen Chen. Self-organized motion in anisotropic swarms. *Journal of Control Theory and Applications*, 1(1):77–81, 2003.

Tianguang Chu, Long Wang, Tongwen Chen, and Shumei Mu. Complex emergent dynamics of anisotropic swarms: Convergence vs oscillation. *Chaos, Solitons & Fractals*, 30(4):875–885, 2006.

Giuseppe Fedele, Luigi D'Alfonso, and Veysel Gazi. A generalized gazi–passino model with coordinate-coupling matrices for swarm formation with rotation behavior. *IEEE Transactions on Control of Network Systems*, 9(3):1227–1237, 2022.

V. Gazi and K. M. Passino. *Swarm Stability and Optimization*. Springer Verlag, January 2011.

Veysel Gazi and Kevin M Passino. A class of attractions/repulsion functions for stable swarm aggregations. *International Journal of Control*, 77(18):1567–1579, 2004.

Jeremy A Goldbogen, Ari S Friedlaender, John Calambokidis, Megan F McKenna, Malene Simon, and Douglas P Nowacek. Integrative approaches to the study of baleen whale diving behavior, feeding performance, and foraging ecology. *BioScience*, 63(2): 90–100, 2013.

Bedir Halcı, Veysel Gazi, and Onur Cihan. Modelling and coordination of a swarm of quadrotors using lagrange dynamics and potential functions. In *2019 24th IEEE International Conference on Emerging Technologies and Factory Automation (ETFA)*, pages 963–970, 2019. doi: 10.1109/ETFA.2019.8869248.

Meng Ji, Giancarlo Ferrari-Trecate, Magnus Egerstedt, and Annalisa Buffa. Containment control in mobile networks. *IEEE Transactions on Automatic Control*, 53(8): 1972–1975, 2008.

Daniela Kengyel, Heiko Hamann, Payam Zahadat, Gerald Radspieler, Franz Wotawa, and Thomas Schmickl. Potential of heterogeneity in collective behaviors: A case study on heterogeneous swarms. In *PRIMA 2015: Principles and Practice of Multi-Agent Systems: 18th International Conference, Bertinoro, Italy, October 26-30, 2015, Proceedings 13*, pages 201–217. Springer, 2015.

Tae-Hyoung Kim and Toshiharu Sugie. Cooperative control for target-capturing task based on a cyclic pursuit strategy. *Automatica*, 43(8):1426–1431, 2007.

Yuichi Kobayashi, Kyouji Otsubo, and Shigeyuki Hosoe. Design of decentralized capturing behavior by multiple mobile robots. In *IEEE Workshop on Distributed Intelligent Systems: Collective Intelligence and Its Applications (DIS'06)*, pages 13–18. IEEE, 2006.

Jianzhen Li, Wei Ren, and Shengyuan Xu. Distributed containment control with multiple dynamic leaders for double-integrator dynamics using only position measurements. *IEEE Transactions on Automatic Control*, 57(6):1553–1559, 2011.

Wim BG Liebrand. The effect of social motives, communication and group size on behaviour in an n-person multi-stage mixed-motive game. *European journal of social psychology*, 14(3):239–264, 1984.

Zhiyun Lin, Mireille Broucke, and Bruce Francis. Local control strategies for groups of mobile autonomous agents. *IEEE Transactions on Automatic Control*, 49(4):622–629, 2004.

Tengfei Liu, Jia Qi, and Zhong-Ping Jiang. Distributed containment control of multi-agent systems with velocity and acceleration saturations. *Automatica*, 117:108992, 2020.

Youcheng Lou and Yiguang Hong. Target containment control of multi-agent systems with random switching interconnection topologies. *Automatica*, 48(5):879–885, 2012.

Joshua Alexander Marshall. *Coordinated autonomy: Pursuit formations of multivehicle systems*. University of Toronto, 2005.

D. Mellinger, N. Michael, and V. Kumar. Trajectory generation and control for precise aggressive maneuvers with quadrotors. *The International Journal of Robotics Research*, 31(5):664–674, 2012.

Alp Merzi and Veysel Gazi. Chemical concentration map building using whale optimization algorithm. In *2017 IEEE Symposium Series on Computational Intelligence (SSCI)*, pages 1–8. Ieee, 2017.

M Alp Merzi, Veysel Gazi, Giuseppe Fedele, Luigi D'Alfonso, and Antonio Bono. Target capturing in an ellipsoidal region with a swarm of quadrotor uavs. In *2022 International Conference on Unmanned Aircraft Systems (ICUAS)*, pages 972–981. IEEE, 2022.

Ryan O Murphy, Kurt A Ackermann, and Michel Handgraaf. Measuring social value orientation. *Judgment and Decision making*, 6(8):771–781, 2011.

Alyssa Pierson, Wilko Schwarting, Sertac Karaman, and Daniela Rus. Weighted buffered voronoi cells for distributed semi-cooperative behavior. In *2020 IEEE International Conference on Robotics and Automation (ICRA)*, pages 5611–5617, 2020a. doi: 10.1109/ICRA40945.2020.9196686.

Alyssa Pierson, Wilko Schwarting, Sertac Karaman, and Daniela Rus. Weighted buffered voronoi cells for distributed semi-cooperative behavior. In *2020 IEEE international conference on robotics and automation (ICRA)*, pages 5611–5617. IEEE, 2020b.

Wei Ren. Consensus tracking under directed interaction topologies: Algorithms and experiments. In *2008 American Control Conference*, pages 742–747. IEEE, 2008.

M. R. Roussel. *Nonlinear Dynamics: A hands-on introductory survey*. Morgan Claypool Publishers, 2019.

Wilko Schwarting, Alyssa Pierson, Javier Alonso-Mora, Sertac Karaman, and Daniela Rus. Social behavior for autonomous vehicles. *Proceedings of the National Academy of Sciences of the United States of America*, 116(50):24972–24978, 2019.

Rodolphe Sepulchre, Derek A Paley, and Naomi Ehrich Leonard. Group coordination and cooperative control of steered particles in the plane. In *Group Coordination and Cooperative Control*, pages 217–232. Springer, 2006.

M. A. Toksöz, S. Oğuz, and V. Gazi. Decentralized formation control of a swarm of quadrotor helicopters. In *15th IEEE International Conference on Control and Automation (ICCA)*, pages 1006–1013. IEEE, 2019.

et al. Walter, Viktor. Uvdar system for visual relative localization with application to leader–follower formations of multirotor uavs. *IEEE Robotics and Automation Letters*, (4.3):2637–2644, 2019.

Viktor Walter, Nicolas Staub, Antonio Franchi, and Martin Saska. Uvdar system for visual relative localization with application to leader–follower formations of multirotor uavs. *IEEE Robotics and Automation Letters*, 4(3):2637–2644, 2019.

Jing Wang. Distributed coordinated tracking control for a class of uncertain multiagent systems. *IEEE Transactions on Automatic Control*, 62(7):3423–3429, 2016.

JINGYI Yao, Raul Ordonez, and Veysel Gazi. Swarm tracking using artificial potentials and sliding mode control. *Journal of Dynamic Systems, Measurement, and Control*, 129(5):749–754, 2007.

Yuanshi Zheng and Long Wang. Distributed consensus of heterogeneous multi-agent systems with fixed and switching topologies. *International Journal of Control*, 85(12): 1967–1976, 2012.

Yuanshi Zheng and Long Wang. Containment control of heterogeneous multi-agent systems. *International Journal of Control*, 87(1):1–8, 2014.